Supporting Information

Materials and Reagents: 4,4',4",4"'-(pyrene-1,3,6,8-tetrayl)tetraaniline (PTBA), 4,4-(1,10-Phenanthroline-2,9-divl)bis[benzaldehyde] (PBBA), and 2,2'-bipyridine-5,5'-dicarbaldehyde (Bpy) were purchased from Bide Pharmatech (Shanghai, China) Ltd. P-toluenethiol, 4-chlorothiophenol, 4-fluorothiophenol, 2-aminobenzenethiol, 3-nitro-benzenethiol, 2-methyl-3-furanthiol, thiophenethiol, 1-propanethiol, allyl mercaptan, 2-methyl-2-propanethiol and cyclohexyl mercaptan were purchased from Aladdin Biochemical Technology (Shanghai, China) Ltd. 2-Methylbenzaldehyde, p-tolualdehyde, 2-fluorobenzaldehyde, 3-chlorobenzaldehyde, 3-bromobenzaldehyde, 4-bromobenzaldehyde, Tempo and benzaldehyde were purchased from Acmec Biochemical (Shanghai, China) Ltd. Indole, 2-methylindole, 5-methylindole, 6-methylindole, 6-fluoroindole, 6-chloroindole, 6-Bromoindole and 1,4-benzoquinone were purchased from Meryer Biochemical Technology (Shanghai, China) Ltd. L-histidine, DMF, acetonitrile, dichloromethane, 1,2-dichloroethane, dimethyl sulfoxide, 1,4-dioxane, hexane, 2,2,4-trimethylpentane, methanol were purchased from Sigma Aldrich Trading (Shanghai, China) Ltd.

Characterization: The crystalline structure of COF was revealed by powder X-ray diffraction (PXRD) with Cu/Kα radiation (D8 AD-VANCE) on a Bruker AVANCE 600M (Germany). Solid-state ^{13}C cross-polarization/magic angle spinning (CP-MAS) spectra were conducted. With an infrared spectrometer (Shimadzu, Thermo Nicolet 380). Fourier transform infrared (FT-IR) spectra with KBr particles at room temperature were obtained. The Brunauer-Emmett-Teller (BET) was performed on a fully automatic

specific surface area and pore size analyzer (ASAP 2460, USA). The X-ray photoelectron spectroscopy (XPS) experiments and morphology (ZEISS) were conducted on a Thermo Escalab 250Xi instrument (Thermo Scientific, USA). Scanning electron microscopy was carried out using a Jeol scanning electron microscope (JSM-7610FPlus, Japan). Meanwhile, the TEM observations were conducted on an FEI Talos F200X transmission electron microscope (USA). In addition, UV–vis diffuse reflectance spectroscopy (DRS) was performed using a Shimadzu UV-3600 instrument (China). The FLS1000/FS5 spectrofluorometer was used to record photoluminescence (PL) spectroscopy and the time-resolved fluorescence decay spectrum (TRPL) at room temperature (US). For the photocurrent measurements, an electrochemical workstation (CHI760E, CH Instruments, China) was used with a standard three-electrode configuration. The electron paramagnetic resonance (EPR) was conducted on a Bruker A300-10/1 instrument (Germany). The ^{1}H NMR and ^{13}C NMR spectra were obtained on a Bruker AV-400 spectrometer using a standard Bruker magic spinning probe. The gas chromatographs and mass spectrometer used was GC–MS (5977A/7890B) manufactured by Agilent, America. The carrier gas is high-purity helium (>99.999%).

Density functional theory (DFT) calculations: All the DFT calculations were performed by using Gaussian 16 package.[1] The geometries optimization calculations were computed by employing the B3LYP functional[2, 3] in conjunction with the 6-31G(d) basis set[4] in the gas phase. The Grimme's DFT-D3 with BJ-damping method was applied to correct the dispersion interaction.[5] The analysis of electronic structure was performed by using Multiwfn 3.8 (dev) code.[6] The isosurface maps of various

orbitals were rendered by means of Visual Molecular Dynamics (VMD) software[7] based on the files exported by Multiwfn. The isosurface of HOMO-LUMO orbitals was set to 0.03. During the quantitative analyses of ESP on vdW surface in Multiwfn program, the grid spacing was set to 0.25 Bohr. The vdW surface referred throughout this paper denotes the isosurface of $\rho = 0.001$ e/bohr^3. [8-9]

Synthesis of PP -COF: PTBA (0.04 mmol), and PBBA (0.08 mmol) were added in a solvent mixture of o-DCB, n-BuOH, and 6 M acetic acid (0.5 mL, 1.5 mL, 0.2 mL) in a 10 mL Pyrex tube. Three freeze-pump-thaw cycles were used to degas the Pyrex tube after it had been placed into an ultrasonic bath for 15 min. The tube was then sealed with a flame and heated to 120 °C for 72 hours. All unreacted monomers were eliminated from the precipitate by filtering it and extracting it with acetone Soxhlet. The powder was then collected and vacuum-dried at 120 °C for a whole night, obtaining the PP-COF as light yellow with a yield of 92%.

Synthesis of 2D PyTTA-COF: A Pyrex tube was charged with PTBA (28.25 mg, 0.5 mmol), Bpy (21 mg, 0.5 mmol), 1 mL of 1,2-Dichlorobenzene and 1 mL of 1-Butanol. After sonication for 10 min, 0.1 mL of acetic acid (6 M) was added into the mixture. The tube was flash frozen at 77 K (liquid N_2 bath), degassed under freeze-pump-thaw for three cycles. The tube was flame sealed and heated at 120 °C for 3 days. These solid at the bottom of the tube which was isolated either by filtration and washed with anhydrous THF and anhydrous acetone, yielding 82%.

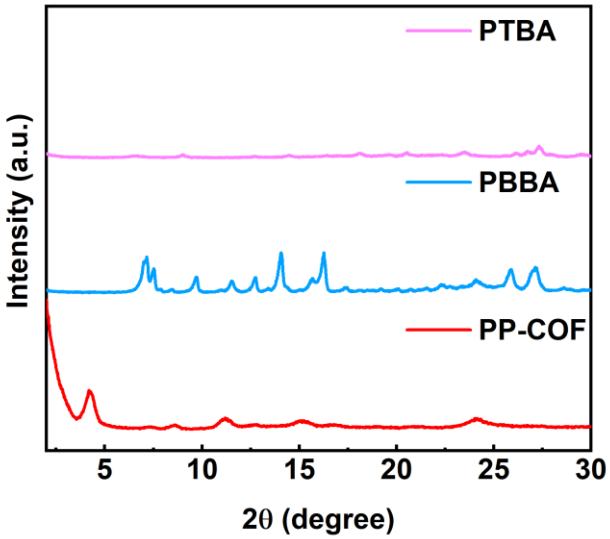

Figure S1. PXRD patterns of PP-COF and ligands.

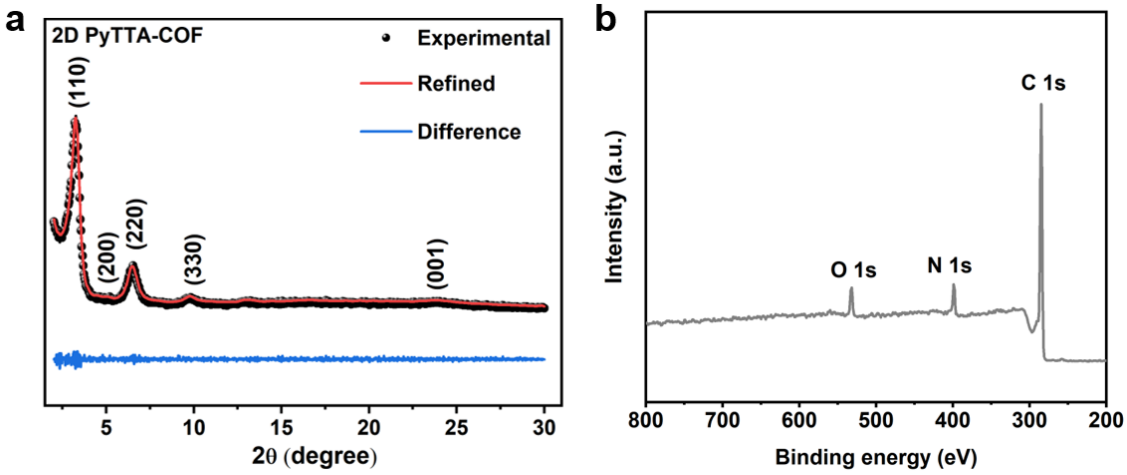

Figure S2. (a) Pawley refinement and experiment pXRD patterns of 2D PyTTA-COF.

(b) XPS survey spectra of PP-COF.

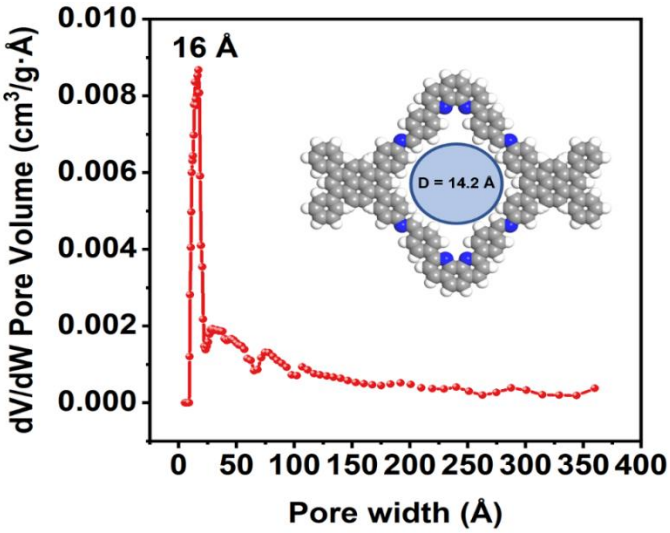

Figure S3. BET pore size distribution of PP-COF.

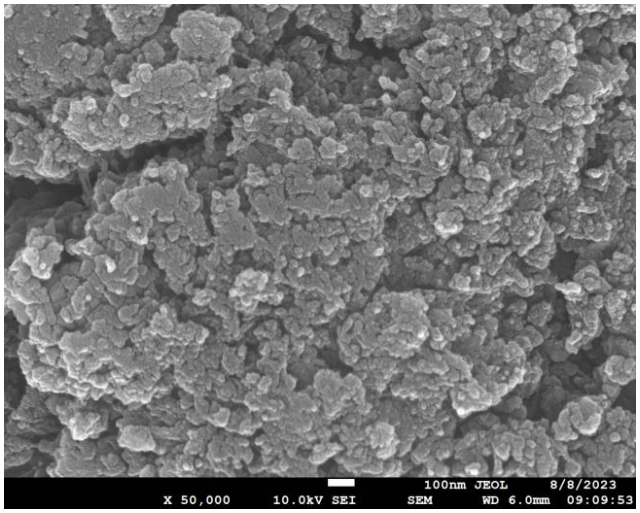

Figure S4. SEM image of PP-COF.

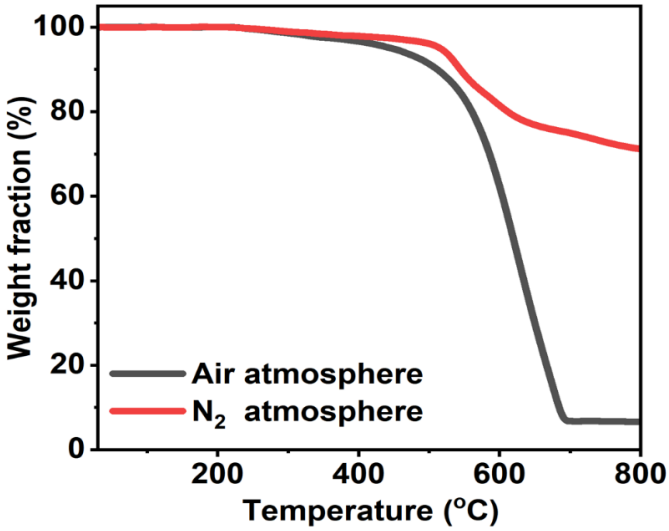

Figure S5. TGA curves of the PP-COF under air or N_2 atmospheres.

Table S1 Synthesis of PP-COF in different solvent conditions.

Entry	Solvent (2.0 mL)	Catalyst	Temperature (°C)	Time (h)
1	o-DCB/n-BuOH = 1/1			
2	Dio/Mes = 1/1	6.0M HOAc	120	72
3	DMAc/Mes = 1/1			

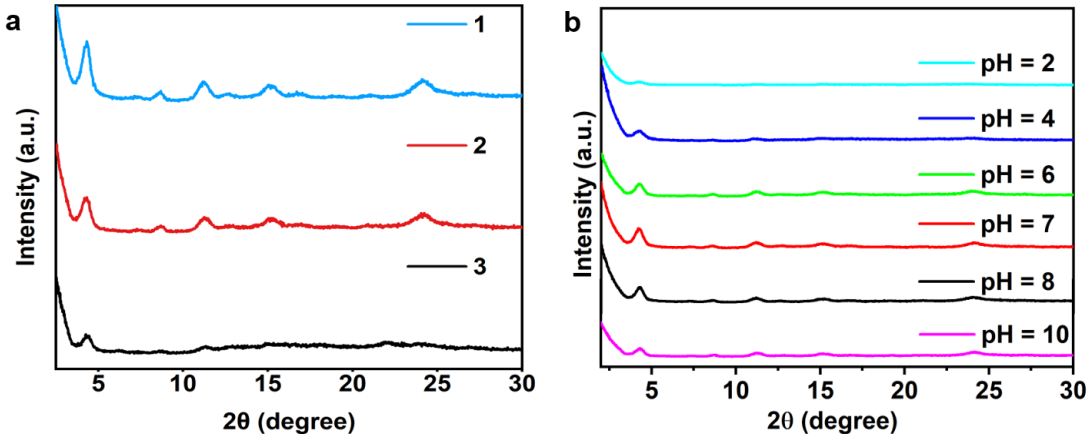

Figure S6. PXRD patterns of PP-COF under (a) different solvent conditions and (b) different pH values.

Table S2 Synthesis of PP-COF in the o-DCB/n-BuOH system with different proportions.

Entry	Solvent (2.0 mL)	Catalyst	Temperature (°C)	Time (h)
1	o-DCB/n-BuOH = 1/9			
2	o-DCB/n-BuOH = 1/6			
3	o-DCB/n-BuOH = 1/3			
4	o-DCB/n-BuOH = 1/1	6.0M HOAc	120	72
5	o-DCB/n-BuOH = 3/1			
6	o-DCB/n-BuOH = 6/1			
7	o-DCB/n-BuOH = 9/1			

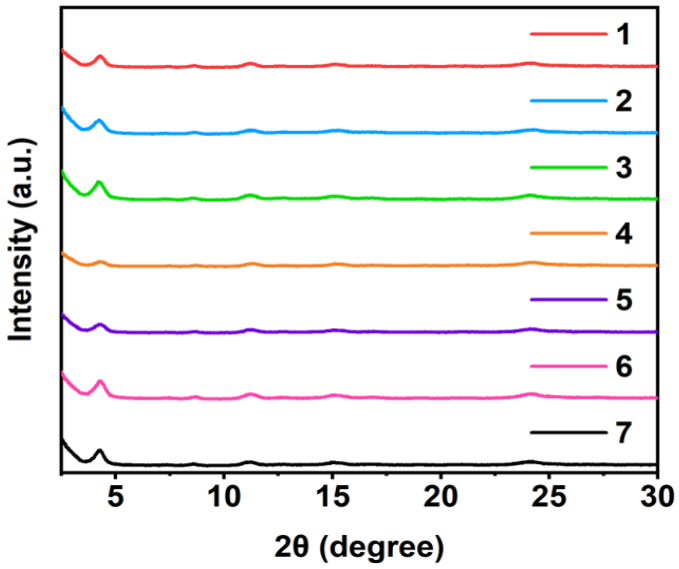

Figure S7. pXRD patterns of PP-COF in the o-DCB/n-BuOH system at different proportions.

Electrochemical measurement

The electrochemical impedance spectra (EIS), Mott-Schottky plot, and transient photocurrent (TPC) were measured using a CHI 660C electrochemical station in a standard three-electrode configuration. The samples (about 10 mg) were mixed with ethanol solution (1 mL) that contained Nafion (50 μL) and then treated with ultrasound for 1 h. The prepared suspension (100 μL) was spin-coated on the FTO glass and then dried at 120 ℃. The FTO substrate obtained served as the working electrode. A saturated Ag/AgCl electrode was used as the reference electrode, and the Pt plate as the counter electrode. As the electrolyte, a 0.5 M Na_2SO_4 solution was employed. A 300 W Xenon lamp with a 420 nm cut-off filter was used as the light source.

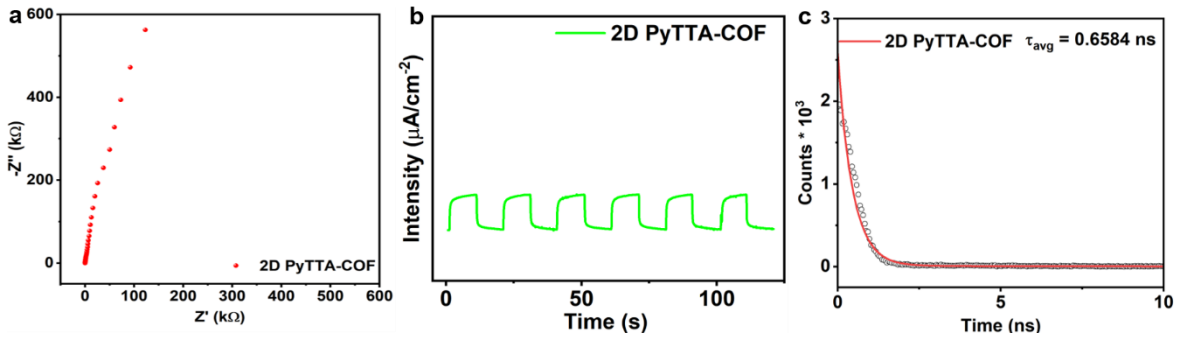

Figure S8. (a) EIS Nyquist plots, (b) Photocurrent response, and (c) TRPL spectra of 2D PyTTA-COF.

Calculation of photoluminescence lifetime

The biexponential model was used to fit the decay profiles:

$$I(t) = A_2 \exp\left(-\frac{t}{\tau_1}\right) + A_2 \exp\left(-\frac{t}{\tau_2}\right) \quad (1)$$

$$\tau = \frac{A_1\tau_1^2 + A_2\tau_2^2}{A_1\tau_1 + A_2\tau_2} \quad (2)$$

where I(t) is intensity, A_1 and A_2 are relative magnitudes, and τ, τ_1 and τ_2 are decay times. By probing the exciton transfer dynamics, the emission decay curves of COFs were fitted by biexponential kinetics function, deriving two decay components, and τ_1 and τ_2 were caused by the nonradiative recombination of charge carriers and the recombination of free excitons, respectively.

Preparation method

Synthesis step: Indoles (0.6 mmol), benzaldehydes (0.2 mmol) and PP-COF (5 mg) were added into 25 mL test tubes containing magnetons and stirred in a photoreaction parallel apparatus (525 nm) at room temperature for 24 h. Following the reaction, an additional 10 ml of ethyl acetate was introduced into the mixture. The aqueous layer underwent two extractions using ethyl acetate. The amalgamated organic solvents were then filtered, combined, and concentrated under vacuum. Subsequently, the residual

was subjected to purification to acquire products **3a-3n**, which exhibited yields ranging from 28% to 98%. This purification process involved the utilization of flash liquid chromatography on silica gel, employing dichloromethane-EtOAc as the extraction solvent.

Synthesis step: Mercaptans (0.5 mmol) and PP-COF (5 mg) were added to a 25 mL test tube containing magnetons, then DMF (3 ml) was added and stirred at room temperature in a photoreaction parallel instrument (465 nm) for 2 h. The same pretreatments were used to obtain products **5a-5k** ranging from 66% to 98% yields.

Reaction mechanism

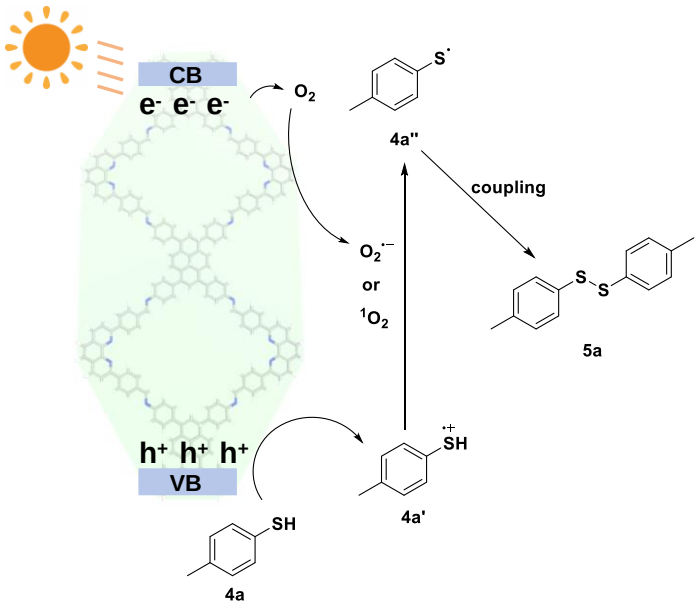

Figure S9. Proposed mechanism of photocatalytic oxidative thiols coupling.

Table S3 Photocatalytic oxidative coupling of *p*-toluenethiol by PP-COF.[a]

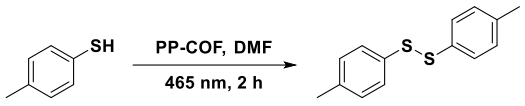

4a 5a

Entry	Catalyst	Solvent	Time (h)	Yield (%)[b]
1	PP-COF	DMF	2 h	98
2	PP-COF	DMSO	2 h	74
3	PP-COF	-	2 h	40
4	PP-COF	Acetonitrile	2 h	n.d.
5	PP-COF	Dichloromethane	2 h	n.d.
6	PP-COF	DCE	2 h	n.d.
7	PP-COF	1,4-Dioxane	2 h	n.d.
8	PP-COF	Hexane	2 h	n.d.
9	PP-COF	2,2,4-Trimethylpentane	2 h	n.d.
10	PTBA	DMF	2 h	34
11	PBBA	DMF	2 h	51
12	-	DMF	2 h	38
13[c]	PP-COF	DMF	2 h	76
14[d]	PP-COF	DMF	2 h	60
15[e]	PP-COF	DMF	2 h	n.d.
16[f]	PP-COF	DMF	2 h	73
17	PP-COF	DMF	1 h	74
18[g]	PP-COF	DMF	2 h	63
19[h]	PP-COF	DMF	2 h	n.d.
20[i]	PP-COF	DMF	2 h	n.d.
21[j]	PP-COF	DMF	2 h	n.d.
22[k]	PP-COF	DMF	2 h	40

[a] Reaction conditions: PP-COF (5.0 mg), *p*-toluenethiol (0.5 mmol), solvent (3.0 mL), under air, 12.0 W blue LED lamp 465 nm, 25 °C.

[b] Isolated yield.

[c] 12.0 W green LED lamp 525 nm.

[d] 12.0 W white LED lamp.

[e] No light irradiation.

[f] The amount of PP-CO was 3 mg.

[g] 8.0 W blue LED lamp 465 nm.

[h] In N_2.

[i] TEMPO (0.5 mmol) as a radical inhibitor.

[j] 1,4-Benzoquinone (0.5 mmol) as a superoxide radical capture.

[k] L-histidine (0.5 mmol) as a singlet oxygen capture.

The reusability of PP-COF for photocatalytic organic conversion

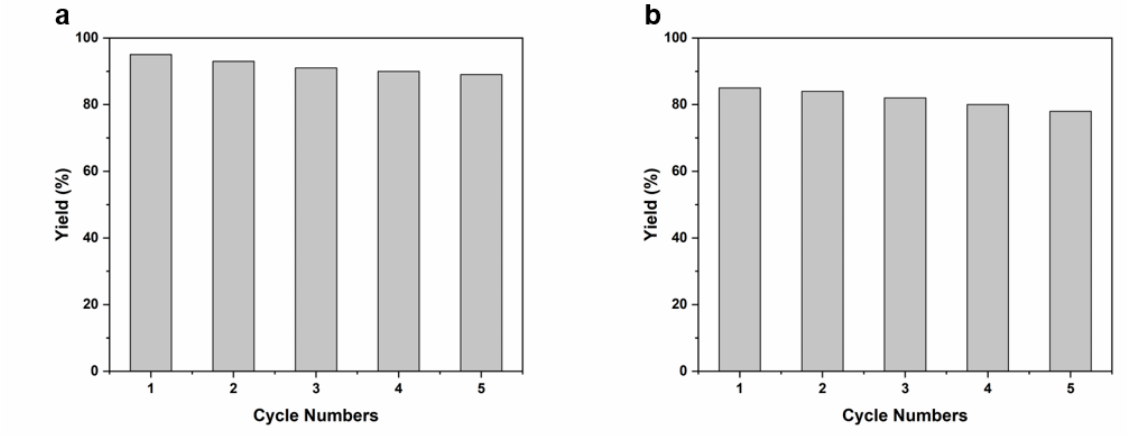

Figure S10. Cycle numbers under optimum conditions. (a) Photocatalytic reaction of indole and benzaldehyde by PP-COF. (b) Photocatalytic oxidative coupling of *p*-toluenethiol by PP-COF.

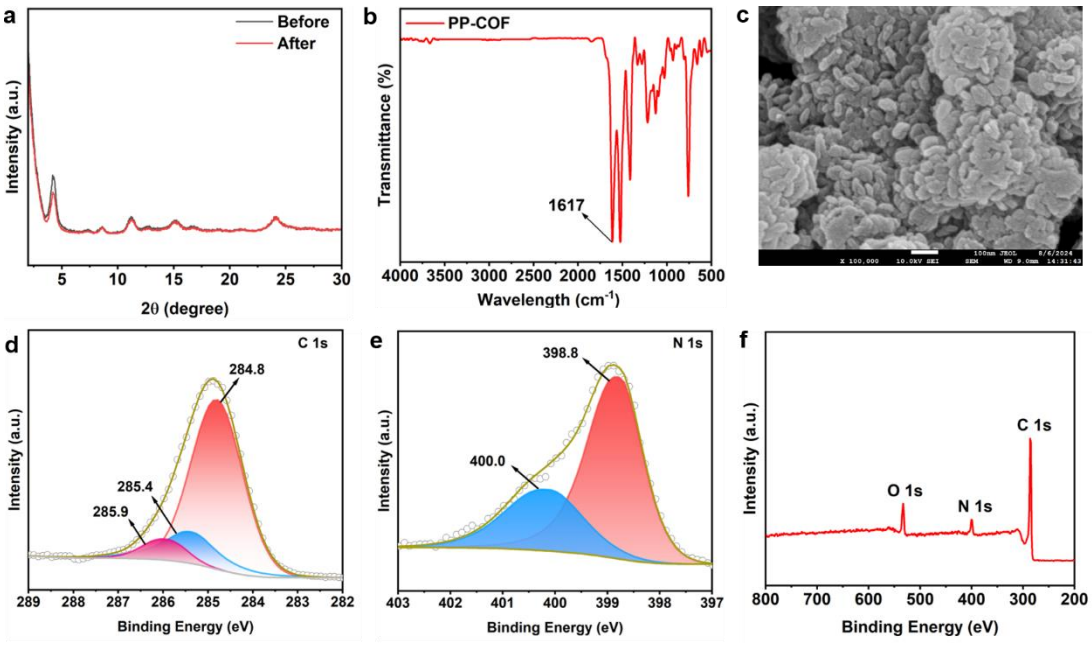

Figure S11. (a) pXRD patterns before and after photocatalytic organic conversion. (b) FTIR spectra, (c) SEM image, (d) C 1s and (e) N 1s spectra, (f) XPS survey spectra of PP-COF after photocatalytic organic conversion.

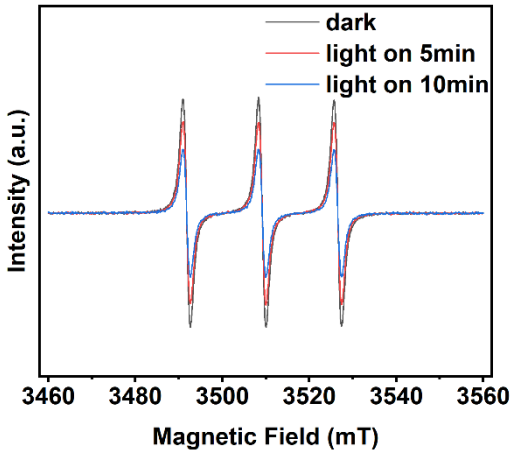

Figure S12. EPR signals of electron-hole (TEMPO-h+) at different times for C-3 functionalization of indole with benzaldehyde. Test conditions are as follows: PP-COF (5.0 mg), indole (0.6 mmol), benzaldehyde (0.2 mmol), under air, 12.0 W green LED lamp 525 nm, 25 °C.

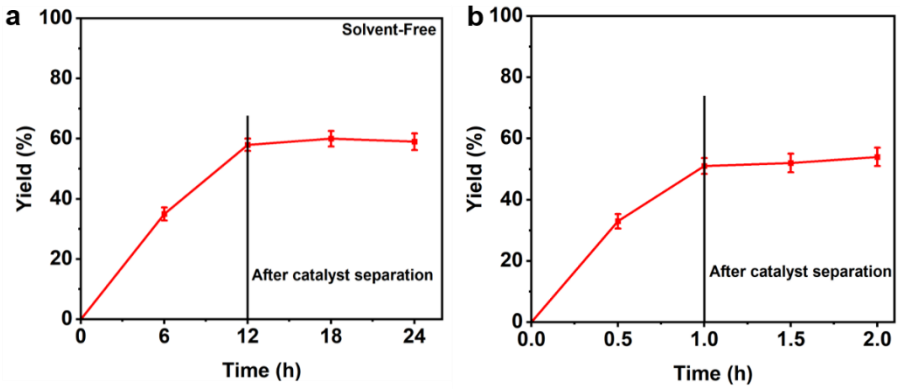

Figure S13. (a) Yield of the leaching test for photocatalytic reaction of indole and benzaldehyde under solvent-free condition. The catalyst was separated by centrifugation at 12 h of the reaction. Reaction conditions are as follows: PP-COF (5.0 mg), indole (0.6 mmol), benzaldehyde (0.2 mmol), under air, 12.0 W green LED lamp 525 nm, 25 °C. (b) Yield of the leaching test for photocatalytic reaction of *p*-toluenethiol using DMF as the solvent. The catalyst was separated by centrifugation at 1 h of the reaction. Reaction conditions are as follows: PP-COF (5.0 mg), *p*-toluenethiol (0.5 mmol), solvent (3.0 mL), under air, 12.0 W blue LED lamp 465 nm, 25 °C.

Table S4 Comparison of photocatalyzed oxidative coupling reaction for representative COFs photocatalysts.

Materials	Light source	Additive	Reaction time (h)	Yield (%)	Ref
$Co(NO_3)_2$/COF (10 mg)	300 W Xe lamp	CH_3CN	6	99	[10]
Por-BC-COF (10 mg)	20 W red LEDs	CH_3CN	1	97	[11]
Por-HZ-COF (5 mg)	12 W red LEDs	MeCN	0.5	86	[12]
PY-BT COF (5 mg)	300 W Xe lamp	CH_3CN	2.5	99	[13]
Py-BSZ-COF (5 mg)	15 W green LEDs	CH_3CN	12	99	[14]
TFB-33-DMTH (10 mg)	30 W blue LEDs	H_2O	20	99	[15]
COF-TpPa (10 mg)	5 W purple LEDs	CH_3CN	8	99	[16]
BTDA-TAPT (6 mg)	300 W Xe lamp	CH_3CN	6	99	[17]
2D PyTTA-COF (5mg)	**12 W green LEDs**	**-**	**24**	**45**	
2D PyTTA-COF (5mg)	**12 W blue LEDs**	**DMF**	**24**	**16**	**This work**
PP-COF (5mg)	**12 W blue LEDs**	**DMF**	**2**	**98**	

Characterization data of catalytic products

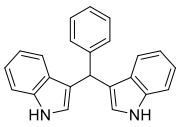

3a[18]: 3,3'-(phenylmethylene)bis(1H-indole): ^{1}H NMR (400 MHz, $CDCl_3$): 7.82 (s, 2H), 7.47 (d, *J* = 8.1 Hz, 2H), 7.35-7.29 (m, 4H), 7.29-7.23 (m, 2H), 7.23-7.17 (m, 1H), 7.15 (td, *J* = 7.1, 1.1 Hz, 2H), 7.03-6.94 (m, 2H), 6.59 (dd, *J* = 2.5, 0.9 Hz, 2H), 5.87 (s, 1H) ppm; ^{13}C NMR (100 MHz, $CDCl_3$): 144.0, 136.7, 128.8, 128.2, 127.1, 126.2, 123.7, 121.9, 119.9, 119.7, 119.2, 111.1, 40.2 ppm.

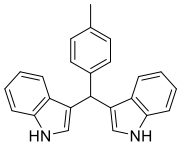

3b[19]: 3,3'-(*p*-tolylmethylene)bis(2-methyl-1H-indole): ^{1}H NMR (400 MHz, $CDCl_3$): 7.84 (s, 2H), 7.38 (d, *J* = 8.0 Hz, 2H), 7.32 (d, *J* = 8.2 Hz, 2H), 7.22-7.18 (m, 2H), 7.15 (td, *J* = 7.2, 1.0 Hz, 2H), 7.07 (d, *J* = 7.9 Hz, 2H), 6.97 (td, *J* = 8.0, 0.9 Hz, 2H), 6.62 (dd, *J* = 2.3, 0.8 Hz, 2H), 5.84 (s, 1H), 2.31 (s, 3H) ppm; ^{13}C NMR (100 MHz, $CDCl_3$): 141.0, 136.7, 135.5, 128.9, 128.6, 127.1, 123.6, 121.9, 119.9, 119.9, 119.2, 111.0, 39.8, 21.1 ppm.

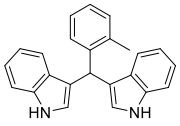

3c[20]: 3,3'-(*o*-tolylmethylene)bis(1H-indole): ^{1}H NMR (400 MHz, $CDCl_3$): 7.78 (s, 2H), 7.39-7.33 (d, *J* = 8.0 Hz, 2H), 7.33 (d, *J* = 8.2 Hz, 2H), 7.22-7.18 (m, 1H), 7.18-7.09 (m, 3H), 7.09-7.04 (m, 1H), 7.04-6.94 (m, 3H), 6.540 (dd, *J* = 2.2, 0.8 Hz, 2H), 6.00 (s, 1H), 2.37 (s, 3H) ppm; ^{13}C NMR (100 MHz, $CDCl_3$): 142.1, 136.7, 136.1, 130.2, 128.4, 127.2, 126.1, 125.9, 123.9, 121.9, 119.8, 119.2, 119.1, 111.1, 36.2, 19.6 ppm.

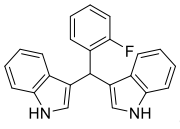

3d[20]: 3,3'-((2-fluorophenyl)methylene)bis(1H-indole): ^{1}H NMR (400 MHz, $CDCl_3$): 7.81 (s, 2H), 7.39 (d, *J* = 8.0 Hz, 2H), 7.30 (d, *J* = 8.2 Hz, 2H), 7.22-7.11 (m, 4H), 7.10-7.02 (m, 1H), 7.03-6.92 (m, 3H), 6.66-6.58 (m, 2H), 6.21 (s, 1H) ppm; ^{13}C NMR (100 MHz, $CDCl_3$): 161.9, 159.5, 136.7, 130.9 (d, *J* = 14.3 Hz), 130.4 (d, *J* = 180.1 Hz), 127.8 (d, *J* = 8.1 Hz), 126.9, 123.9 (d, *J* = 3.5 Hz), 123.6, 122.0,

119.6 (d, *J* = 49.5 Hz), 118.3, 115.3 (d, *J* = 22.1 Hz), 111.1, 32.5 (d, *J* = 4.0 Hz) ppm.

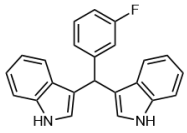

3e[21]: 3,3'-((3-fluorophenyl)methylene)bis(1H-indole): ^{1}H NMR (400 MHz, $CDCl_3$): 7.62 (s, 2H), 7.34 (d, *J* = 8.2 Hz, 2H), 7.24 (d, *J* = 8.1 Hz 2H), 7.21-7.11 (m, 3H), 7.11-7.06 (m, 1H), 7.05-6.94 (m, 3H), 6.92-6.84 (m, 1H), 6.47 (d, *J* = 1.6 Hz, 2H), 5.82 (s, 1H) ppm; ^{13}C NMR (100 MHz, $CDCl_3$): 164.3, 161.8, 144.9 (d, *J* = 6.6 Hz), 136.7, 129.7 (d, *J* = 8.1 Hz), 126.9, 124.5 (d, *J* = 2.6 Hz), 123.7, 122.1, 119.6 (d, *J* = 41.6 Hz), 118.9, 115.6 (d, *J* = 21.4 Hz), 113.2 (d, *J* = 21.1 Hz), 111.3, 40.0 (d, *J* = 1.2 Hz) ppm.

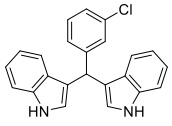

3f[20]: 3,3'-((3-chlorophenyl)methylene)bis(1H-indole): ^{1}H NMR (400 MHz, $CDCl_3$): 7.84 (s, 2H), 7.36 (d, *J* = 8.1 Hz, 2H), 7.34-7.22 (m, 3H), 7.23-7.12 (m, 5H), 7.00 (td, *J* = 8.1, 0.9 Hz, 2H), 6.58 (dd, *J* = 2.4, 1.0 Hz, 2H), 5.83 (s, 1H) ppm; ^{13}C NMR (100 MHz, $CDCl_3$): 146.3, 136.7, 134.1, 129.5, 128.8, 126.9, 126.8, 126.5, 123.7, 122.1, 119.8, 119.4, 118.9, 111.2, 39.9 ppm.

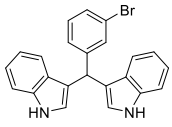

3g[19]: 3,3'-((3-bromophenyl)methylene)bis(1H-indole): ^{1}H NMR (400 MHz, $CDCl_3$): 7.82 (s, 2H), 7.47 (t, *J* = 1.7 Hz, 1H), 7.35 (d, *J* = 8.1 Hz, 2H), 7.34-7.28 (m, 3H), 7.26-7.22 (m, 1H), 7.18 (td, *J* = 8.0, 1.0 Hz, 2H), 7.10 (t, *J* = 7.8 Hz, 1H), 6.98 (td, *J* = 8.0, 0.9 Hz, 2H), 6.55 (dd, *J* = 2.4, 1.0 Hz, 2H), 5.82 (s, 1H) ppm; ^{13}C NMR (100 MHz, $CDCl_3$): 146.6, 136.7, 131.7, 129.9, 129.4, 127.4, 126.9, 123.7, 122.4, 122.1, 119.8, 119.4, 118.9, 111.2, 39.9 ppm.

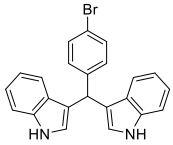

3h[21]: 3,3'-((4-bromophenyl)methylene)bis(1H-indole): ^{1}H NMR (400 MHz, $CDCl_3$): 7.92 (s, 2H), 7.42-7.37 (m, 2H), 7.37-7.31 (m, 4H), 7.24-7.19 (m, 2H), 7.19-7.13 (m, 2H), 7.06-6.97 (m, 2H), 6.62 (dd, *J* = 2.4, 1.1 Hz, 2H), 5.84 (s, 1H) ppm; ^{13}C NMR (100 MHz, $CDCl_3$): 143.1, 136.7, 131.3, 130.5, 126.9, 123.6, 122.1, 119.9,

119.8, 119.4, 119.1, 111.1, 39.7 ppm.

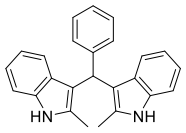

3i[22]: 3,3'-(phenylmethylene)bis(2-methyl-1H-indole): ^{1}H NMR (400 MHz, $CDCl_3$): 7.73 (s, 2H), 7.32-7.26 (m, 2H), 7.26-7.16 (m, 5H), 7.07-6.99 (m, 2H), 6.97 (d, *J* = 7.9 Hz, 2H), 6.88-6.81 (m, 2H), 6.00 (s, 1H), 2.06 (s, 6H) ppm; ^{13}C NMR (100 MHz, $CDCl_3$): 143.7, 135.0, 131.8, 129.1, 128.9, 128.1, 125.9, 120.6, 119.3, 119.1, 113.4, 109.9, 39.3, 12.4 ppm.

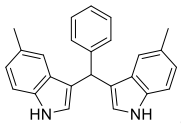

3j[22]: 3,3'-(phenylmethylene)bis(5-methyl-1H-indole): ^{1}H NMR (400 MHz, $CDCl_3$): 7.70 (s, 2H), 7.37-7.29 (m, 2H), 7.29-7.22 (m, 2H), 7.22-7.15 (m, 5H), 6.97 (dd, *J* = 8.2, 1.4 Hz, 2H), 6.51 (dd, *J* = 2.3, 0.8 Hz, 2H), 5.81 (s, 1H), 2.33 (s, 6H) ppm; ^{13}C NMR (100 MHz, $CDCl_3$): 144.2, 135.1, 128.7, 128.4, 128.2, 127.4, 126.1, 123.9, 123.6, 119.5, 119.3, 110.7, 40.1, 21.5 ppm.

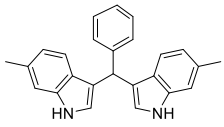

3k[23]: 3,3'-(phenylmethylene)bis(6-methyl-1H-indole): ^{1}H NMR (400 MHz, $CDCl_3$): 7.69 (s, 2H), 7.37-7.29 (m, 2H), 7.29-7.21 (m, 4H), 7.21-7.16 (m, 1H), 7.10 (s, 2H), 6.82 (dd, *J* = 8.1, 0.8 Hz, 2H), 6.52 (dd, *J* = 2.4, 1.1 Hz, 2H), 5.81 (s, 1H), 2.42 (s, 6H) ppm; ^{13}C NMR (100 MHz, $CDCl_3$): 144.2, 137.2, 131.7, 128.7, 128.2, 126.1, 125.0, 122.1, 120.1, 119.6, 119.6, 111.0, 40.3, 21.7 ppm.

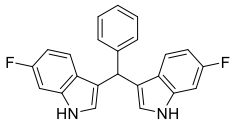

3l[24]: 3,3'-(phenylmethylene)bis(6-fluoro-1H-indole): ^{1}H NMR (400 MHz, $CDCl_3$): 7.90 (s, 2H), 7.35-7.26 (m, 4H), 7.26-7.18 (m, 3H), 7.01 (dd, *J* = 9.6, 2.3 Hz, 2H), 6.81-6.70 (m, 2H), 6.65-6.58 (m, 2H), 5.79 (s, 1H) ppm; ^{13}C NMR (100 MHz, $CDCl_3$): 161.1, 158.8, 136.6 (d, *J* = 12.3 Hz), 128.5 (d, *J* = 26.9 Hz), 126.4, 123.8 (d, *J* = 3.5 Hz), 126.6, 120.6 (d, *J* = 9.9 Hz), 119.6, 108.1 (d, *J* = 24.2 Hz), 97.4 (d, *J* = 25.9 Hz), 40.2 ppm.

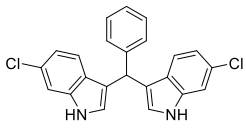

3m[20]: 3,3'-(phenylmethylene)bis(6-chloro-1H-indole): ^{1}H NMR (400 MHz, $CDCl_3$): 7.93 (s, 2H), 7.32 (d, *J* = 1.6 Hz, 2H), 7.31-7.25 (m, 4H), 7.25-7.19 (m, 3H), 6.95 (dd, *J* = 8.5, 1.8 Hz, 2H), 6.61 (dd, *J* = 2.4, 1.1 Hz, 2H), 5.79 (s, 1H) ppm; ^{13}C NMR (100 MHz, $CDCl_3$): 143.4, 137.0, 128.6, 128.4, 127.9, 126.5, 125.6, 124.2, 120.7, 120.1, 119.6, 111.0, 40.1 ppm.

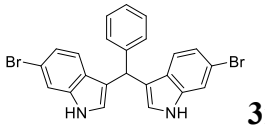

3n[23]: 3,3'-(phenylmethylene)bis(6-bromo-1H-indole): ^{1}H NMR (400 MHz, $CDCl_3$): 8.01 (s, 2H), 7.50 (d, *J* = 1.4 Hz, 2H), 7.38-7.27 (m, 4H), 7.25-7.21 (m, 1H), 7.21 (d, *J* = 8.5 Hz, 2H), 7.12-7.05 (m, 2H), 6.70-6.56 (m, 2H), 5.79 (s, 1H) ppm; ^{13}C NMR (100 MHz, $CDCl_3$): 143.3, 137.5, 128.6, 128.4, 126.4, 125.9, 124.1, 122.7, 121.1, 119.6, 115.6, 114.0, 40.0 ppm.

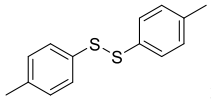

5a[25]: 4-methylphenyl disulfide: ^{1}H NMR (400 MHz, $CDCl_3$): 7.38 (d, *J* = 8.2 Hz, 4H), 7.10 (d, *J* = 8.1 Hz, 4H), 2.31 (s, 6H) ppm; ^{13}C NMR (100 MHz, $CDCl_3$): 137.5, 133.9, 129.8, 128.6, 21.1 ppm.

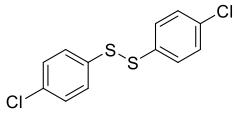

5b[26]: 4-chlorophenyl disulfide: ^{1}H NMR (400 MHz, $CDCl_3$): 7.44-7.35 (m, 4H), 7.31-7.24 (m, 4H) ppm; ^{13}C NMR (100 MHz, $CDCl_3$): 135.2,133.7, 129.4, 129.3 ppm.

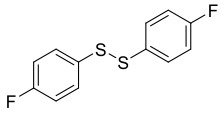

5c[25]: Di-4-fluorophenyl sulfide: ^{1}H NMR (400 MHz, $CDCl_3$): 7.47-7.41 (m, 4H), 7.05-6.95 (m, 4H) ppm; ^{13}C NMR (100 MHz, $CDCl_3$): 162.6 (d, *J* = 246.6 Hz), 132.2 (d, *J* = 3.4 Hz), 131.3 (d, *J* = 8.3 Hz), 116.29 (d, *J* = 22.1 Hz) ppm.

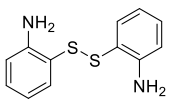

5d[27]: 2,2'-dithiobis(aniline): ^{1}H NMR (400 MHz, $CDCl_3$): 7.21-7.09 (m, 4H), 6.74-6.66 (td, *J* = 7.5, 1.3 Hz, 2H), 6.69 (td, *J* = 7.6, 1.4 Hz, 2H), 4.32 (s, 4H) ppm; ^{13}C NMR (100 MHz, $CDCl_3$): 148.6, 136.9, 131.6, 118.8, 118.3, 115.3 ppm.

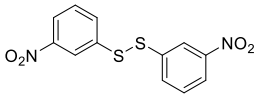

5e[28]: Bis(3-nitrophenyl) persulfide: ^{1}H NMR (400 MHz, $CDCl_3$): 8.37 (t, *J* = 2.0 Hz, 2H), 8.10 (dd, *J* = 8.2, 1.3Hz, 2H), 7.81 (dd, *J* = 7.9, 0.8 Hz, 2H), 7.53 (t, *J* = 8.0 Hz, 2H) ppm; ^{13}C NMR (100 MHz, $CDCl_3$): 148.9, 138.5, 132.8, 130.2, 122.3, 121.9 ppm.

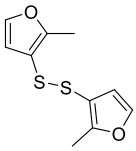

5f[29]: Bis(2-methylfuryl) disulfide: ^{1}H NMR (400 MHz, $CDCl_3$): 7.27 (d, *J* = 2.0 Hz, 2H), 6.37 (d, *J* = 2.0 Hz, 2H), 2.10 (s, 6H) ppm; ^{13}C NMR (100 MHz, $CDCl_3$): 157.0, 140.8, 114.8, 112.7, 11.4 ppm.

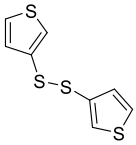

5g[30]: 2-thienyl: ^{1}H NMR (400 MHz, $CDCl_3$): 7.49 (dd, *J* = 5.3, 1.3 Hz, 2H), 7.15 (dd, *J* = 3.6, 1.3 Hz, 2H), 7.05-6.98 (m, 2H) ppm; ^{13}C NMR (100 MHz, $CDCl_3$): 135.7, 135.6, 132.29, 127.78 ppm.

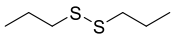

5h[27]: 4,5-dithiaoctane: ^{1}H NMR (400 MHz, $CDCl_3$): 2.67 (t, *J* = 7.2, Hz 4H), 1.77-1.65 (m, 4H), 0.99 (t, *J* = 7.4 Hz, 6H) ppm; ^{13}C NMR (100 MHz, $CDCl_3$): 41.2, 22.5, 13.1 ppm.

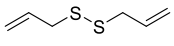

5i[31]: Di-2-propenyl Disulfide: ^{1}H NMR (400 MHz, $CDCl_3$): 5.96-5.70 (m, 2H), 5.31-5.04 (m, 4H), 3.55-3.47 (m, 1H), 3.34 (d, *J* = 7.4 Hz, 2H), 3.09 (dt, *J* = 7.1, 1.1 Hz, 1H) ppm; ^{13}C NMR (100 MHz, $CDCl_3$): 133.5, 118.4, 42.3 ppm.

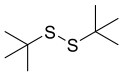

5j[32]: Bis(1,1-dimethylethyl) persulfide: ^{1}H NMR (400 MHz, $CDCl_3$): 1.31 (s, 18H) ppm; ^{13}C NMR (100 MHz, $CDCl_3$): 46.1, 30.6 ppm.

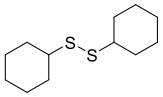

5k[33]: Bis(cyclohexyl)disulfide: ^{1}H NMR (400 MHz, $CDCl_3$): 2.78-2.60 (m, 2H), 2.14-1.96 (m, 4H), 1.87-1.69 (m, 4H), 1.70-1.57 (m, 2H), 1.41-1.16 (m, 10H) ppm; ^{13}C NMR (100 MHz, $CDCl_3$): 49.9, 32.9, 26.1, 25.7 ppm.

NMR spectra of catalytic products

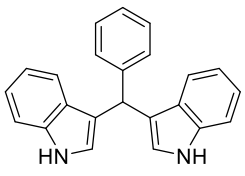

3a

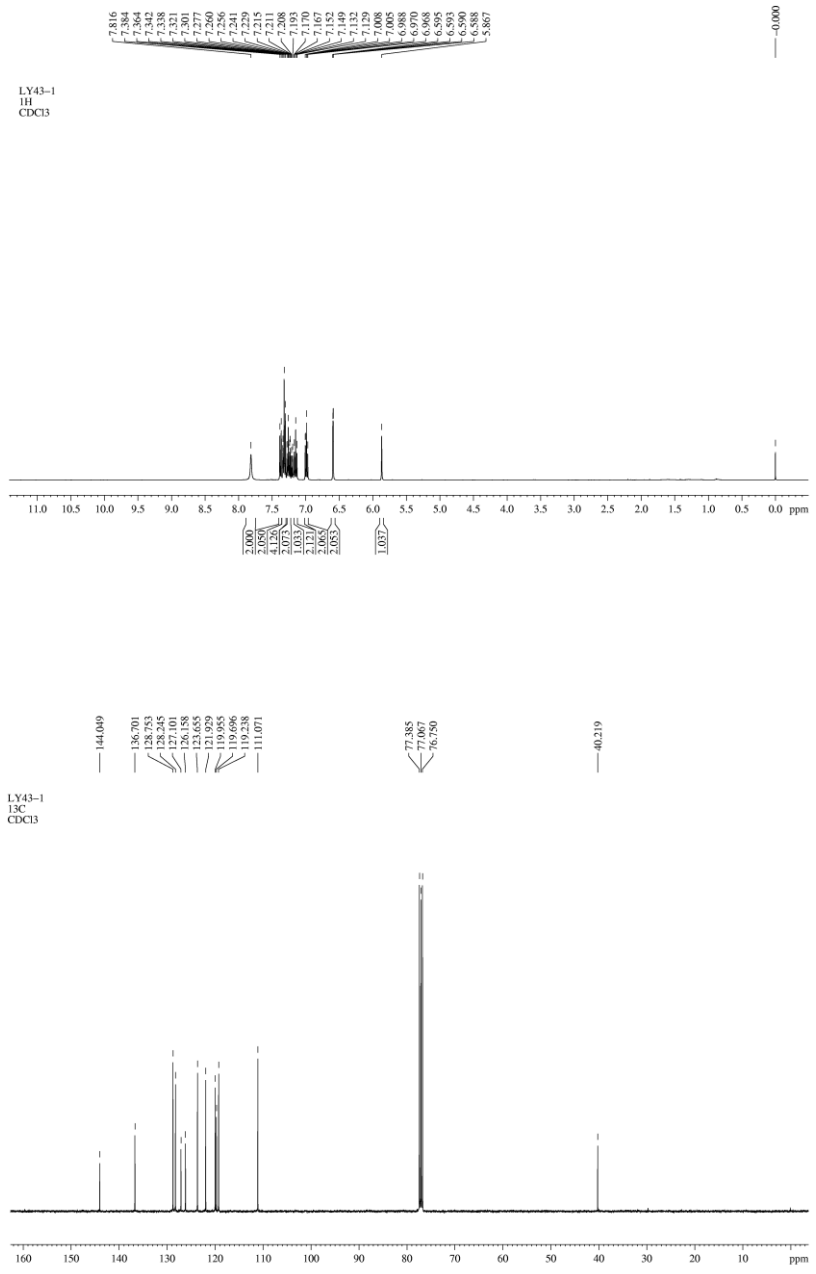

The ^{1}H-NMR and ^{13}C-NMR spectra of 3,3'-(phenylmethylene)bis(1H-indole)

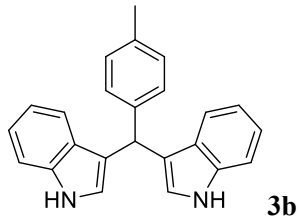

3b

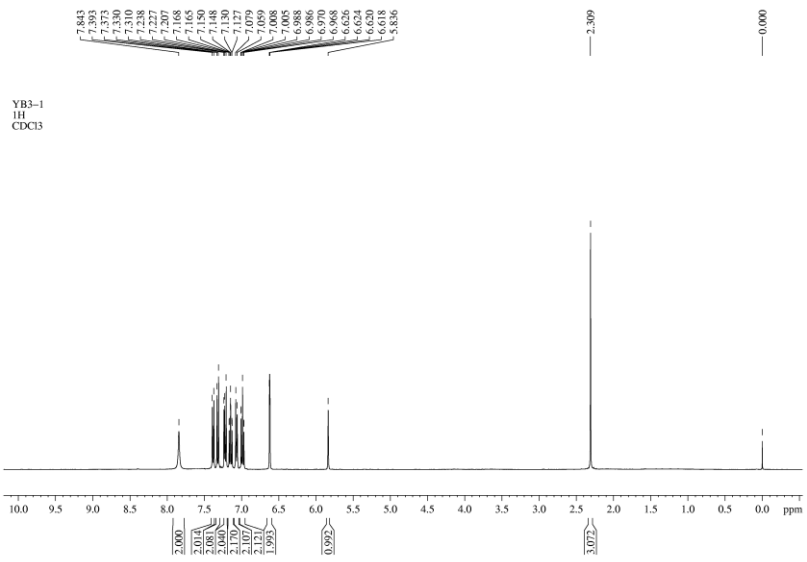

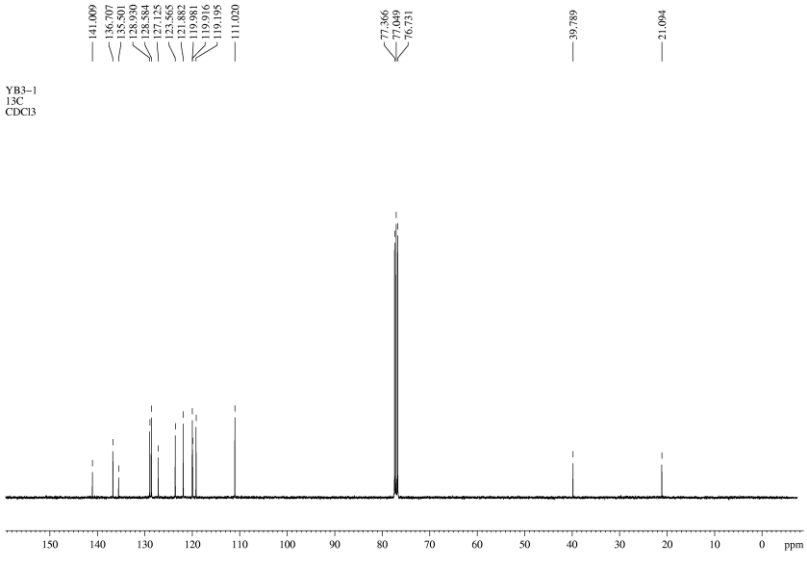

The ^{1}H-NMR and ^{13}C-NMR spectra of 3,3'-(p-tolylmethylene)bis(2-methyl-1H-indole)

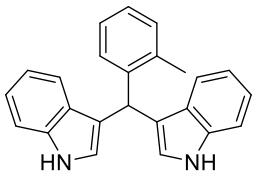

3c

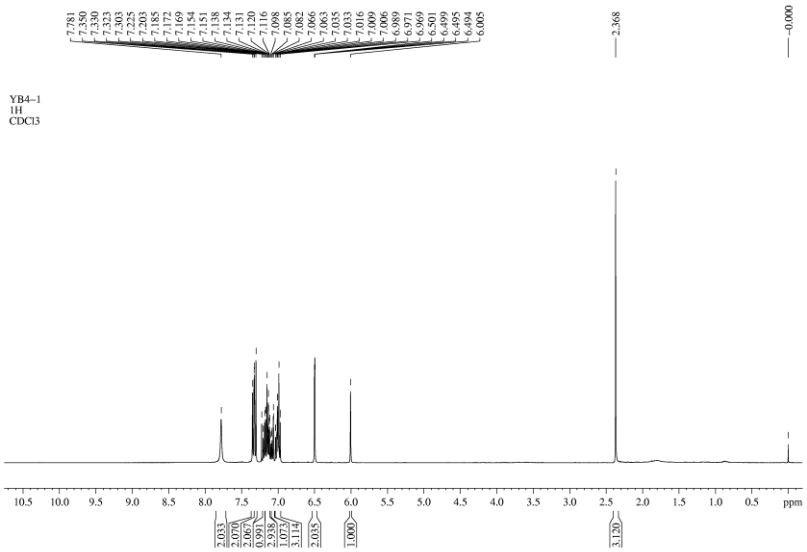

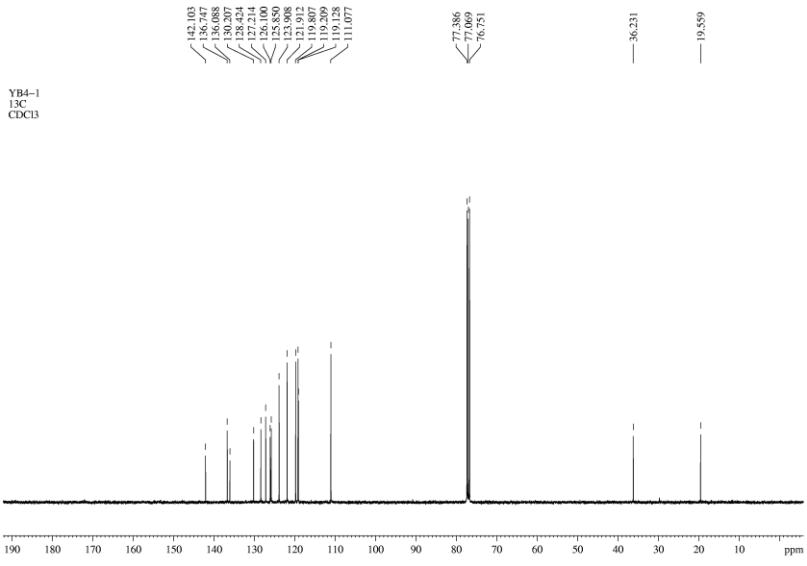

The ^{1}H-NMR and ^{13}C-NMR spectra of 3,3'-(o-tolylmethylene)bis(1H-indole)

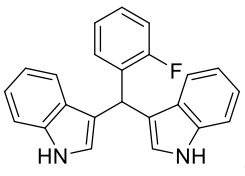

3d

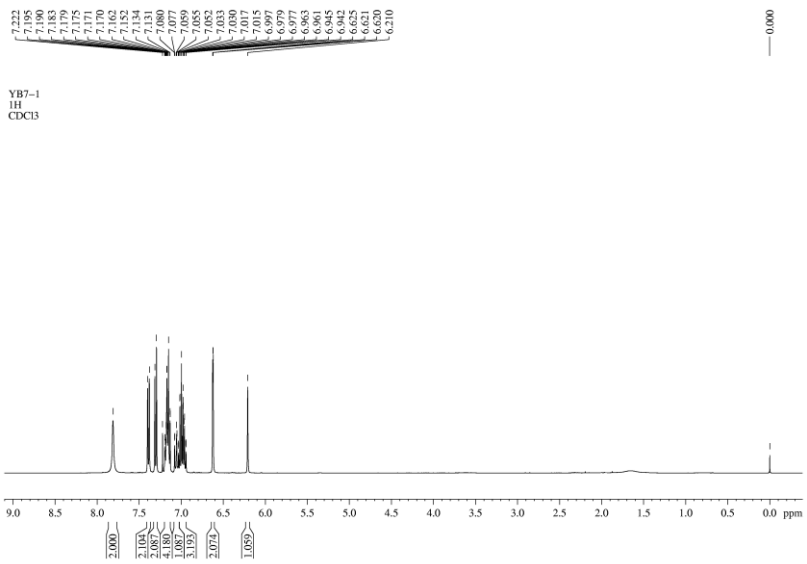

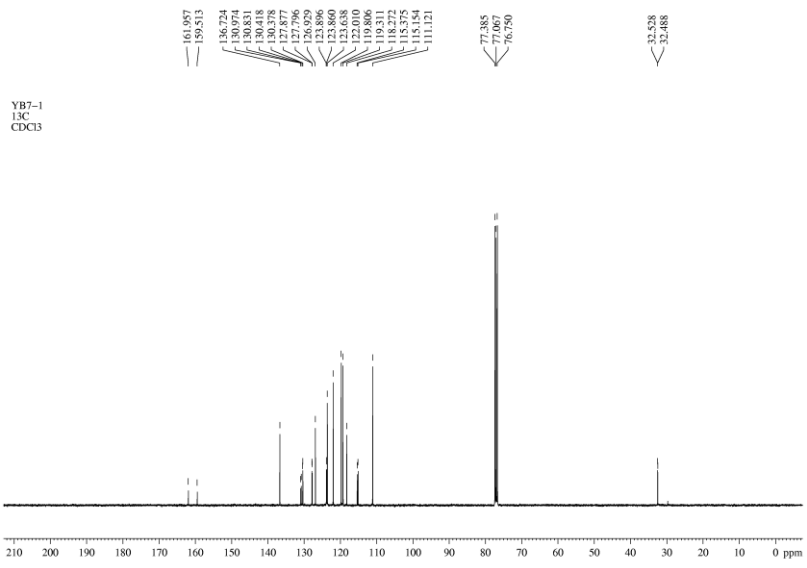

The ^{1}H-NMR and ^{13}C-NMR spectra of 3,3'-((2-fluorophenyl)methylene)bis(1H-indole)

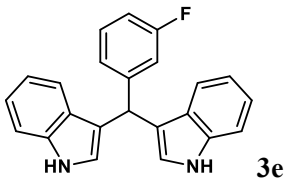

3e

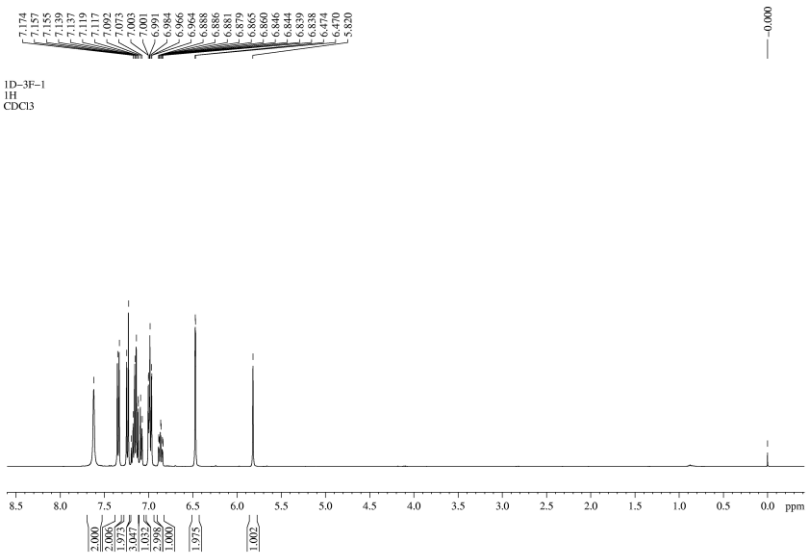

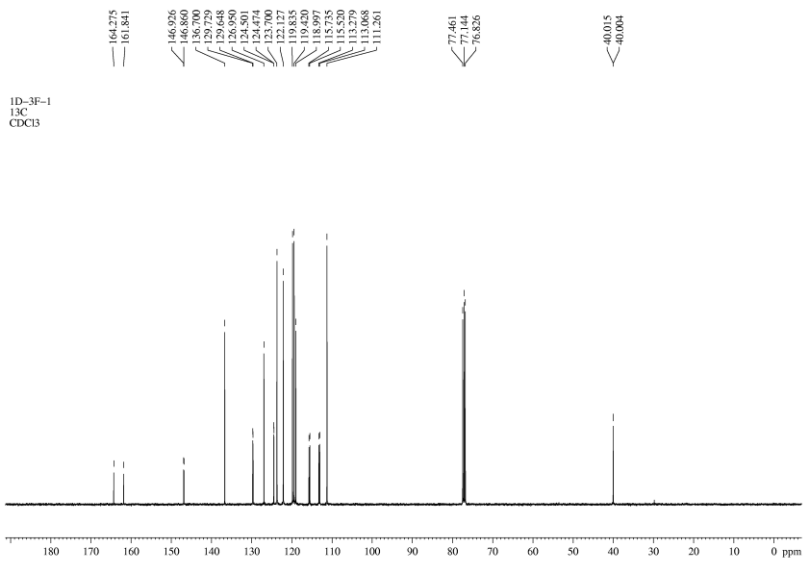

The ^{1}H-NMR and ^{13}C-NMR spectra of 3,3'-((3-fluorophenyl)methylene)bis(1H-indole)

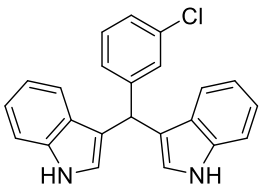

3f

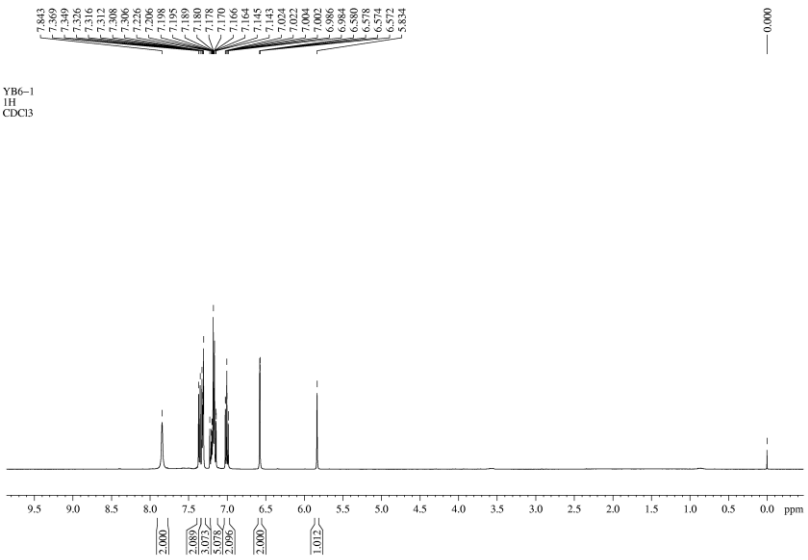

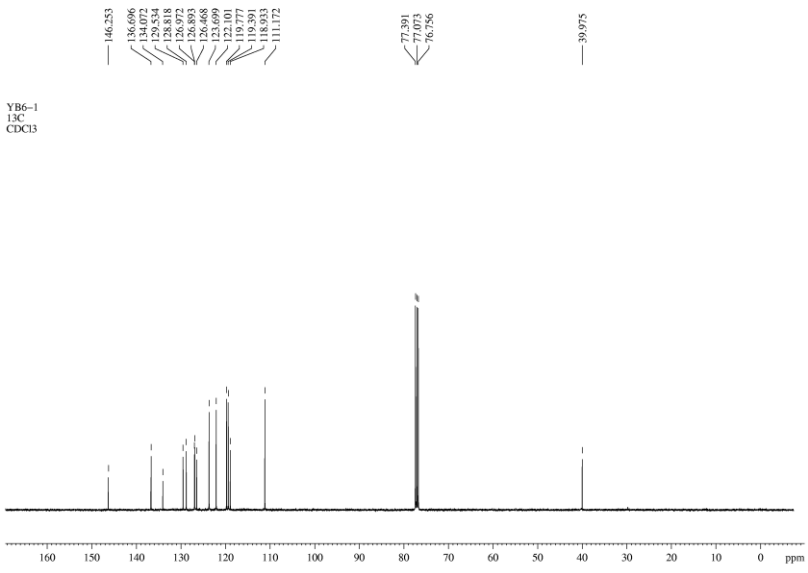

The ^{1}H-NMR and ^{13}C-NMR spectra of 3,3'-((3-chlorophenyl)methylene)bis(1H-indole)

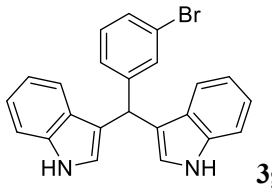

3g

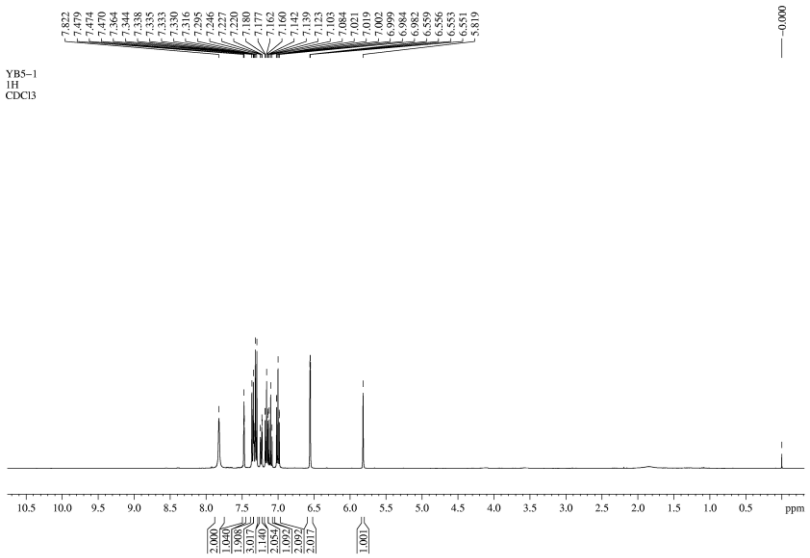

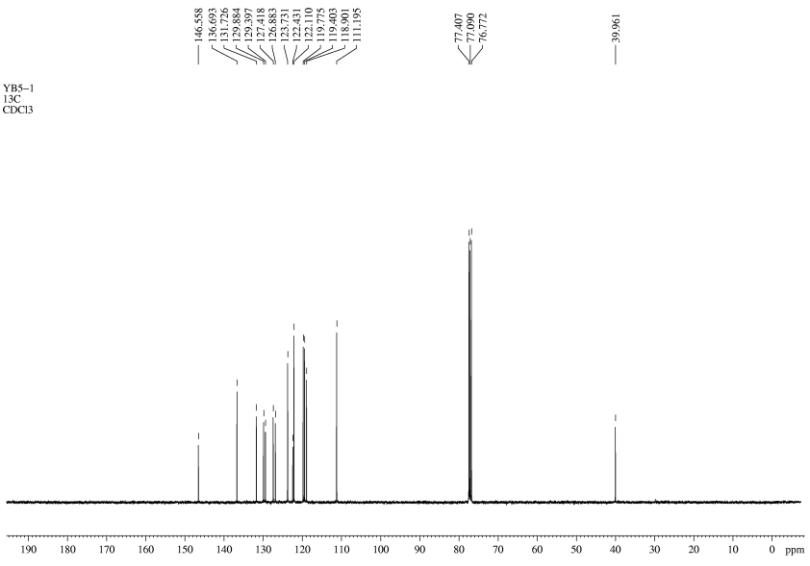

The ^{1}H-NMR and ^{13}C-NMR spectra of 3,3'-((3-bromophenyl)methylene)bis(1H-indole)

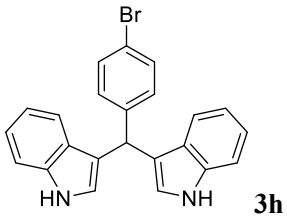

3h

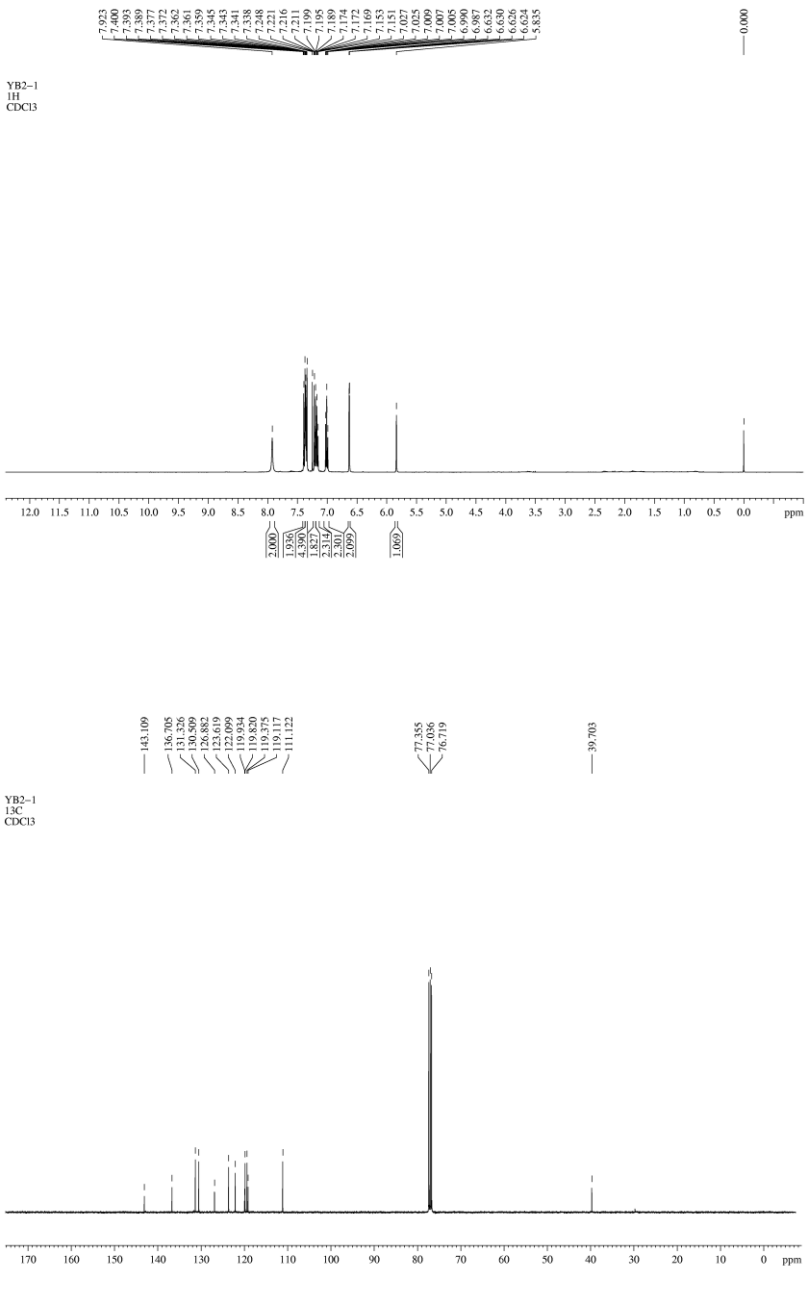

The ^{1}H-NMR and ^{13}C-NMR spectra of 3,3'-((4-bromophenyl)methylene)bis(1H-indole)

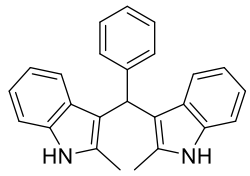

3i

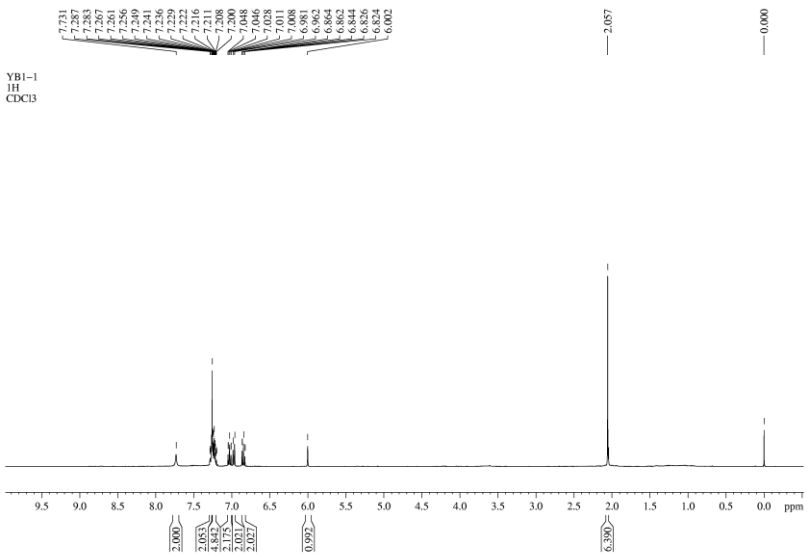

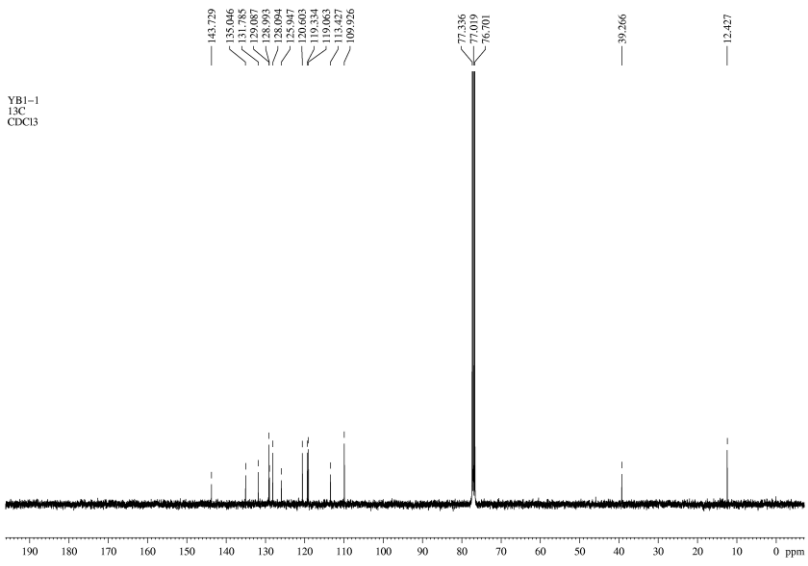

The ^{1}H-NMR and ^{13}C-NMR spectra of 3,3'-(phenylmethylene)bis(2-methyl-1H-indole)

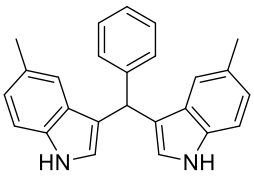

3j

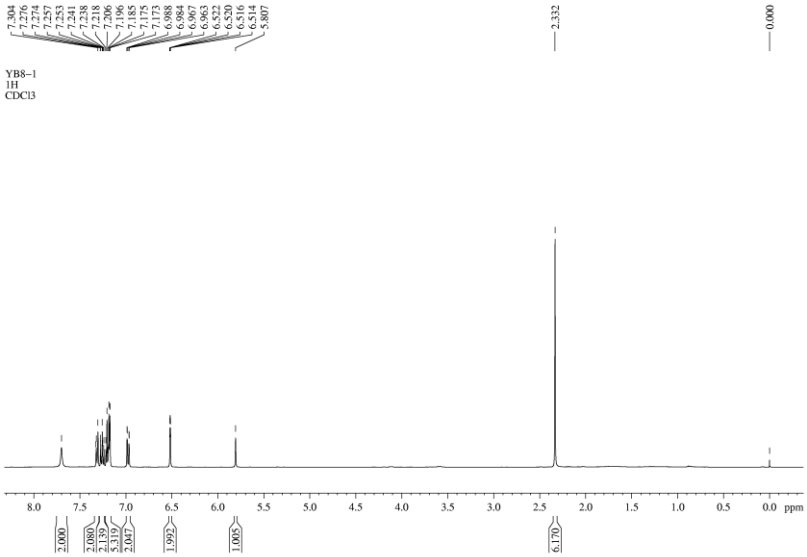

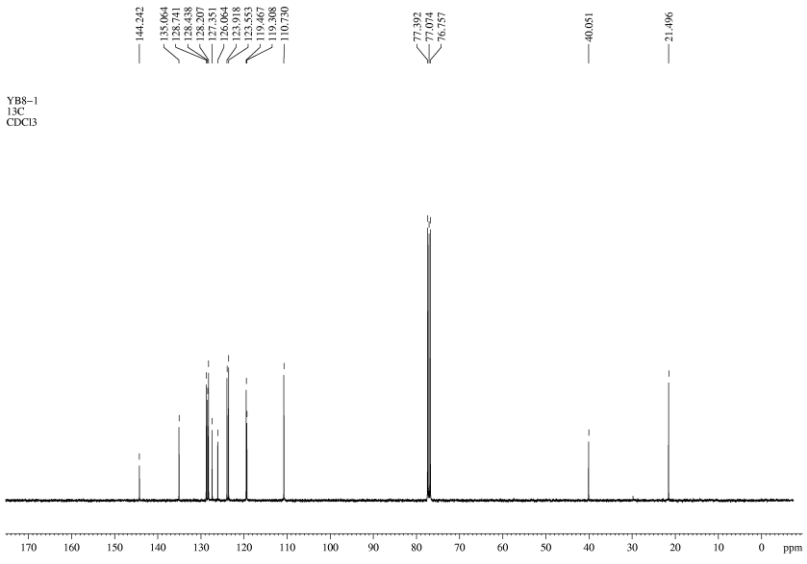

The ^{1}H-NMR and ^{13}C-NMR spectra of 3,3'-(phenylmethylene)bis(5-methyl-1H-indole)

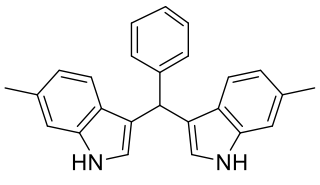

3k

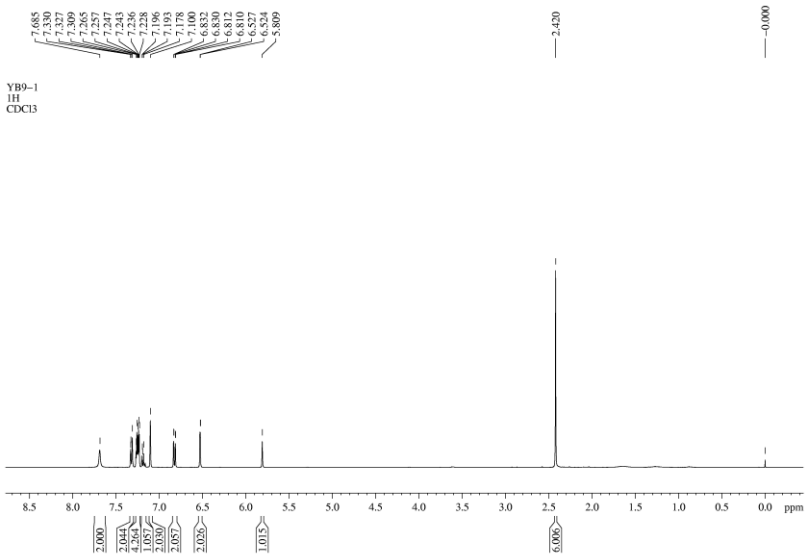

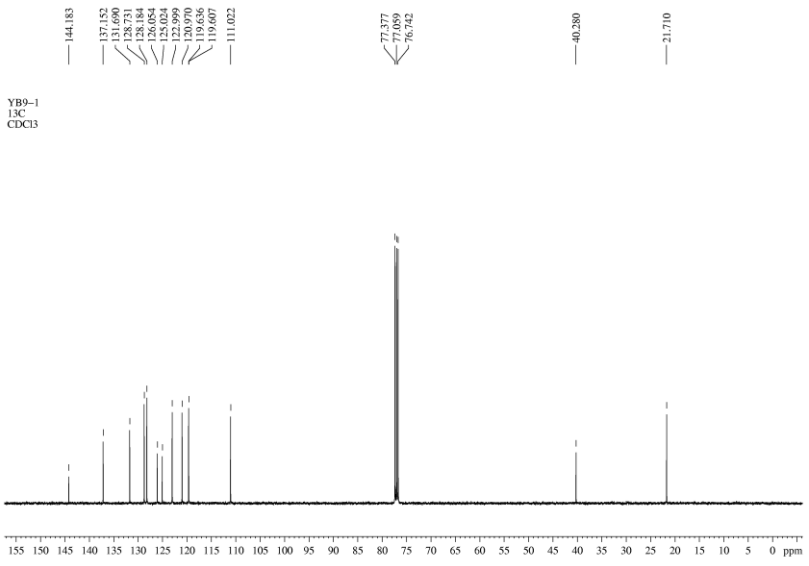

The ^{1}H-NMR and ^{13}C-NMR spectra of 3,3'-(phenylmethylene)bis(6-methyl-1H-indole)

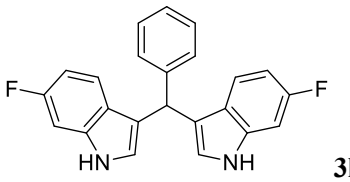

3l

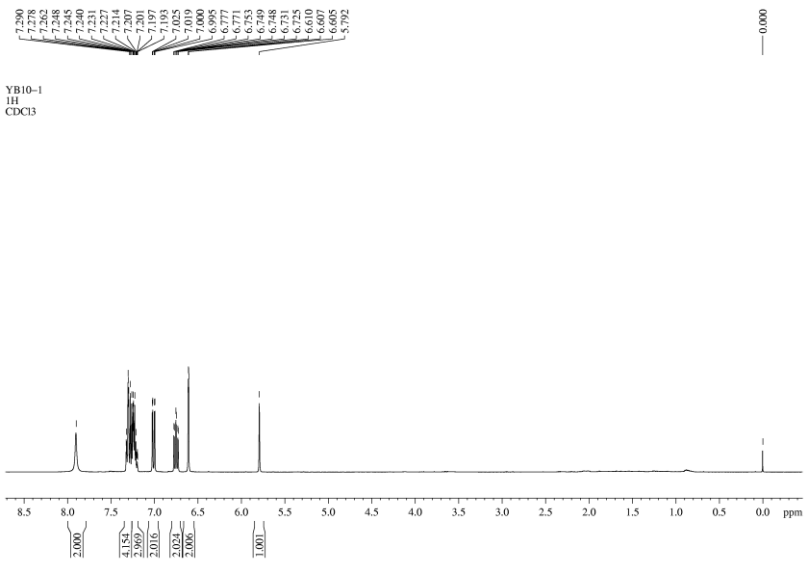

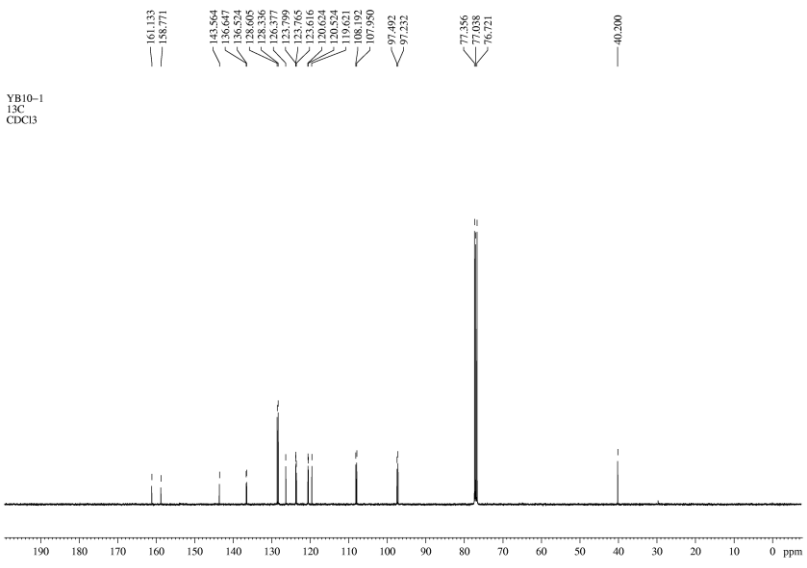

The ^{1}H-NMR and ^{13}C-NMR spectra of 3,3'-(phenylmethylene)bis(6-fluoro-1H-indole)

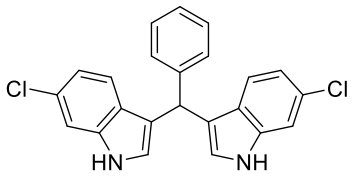

3m

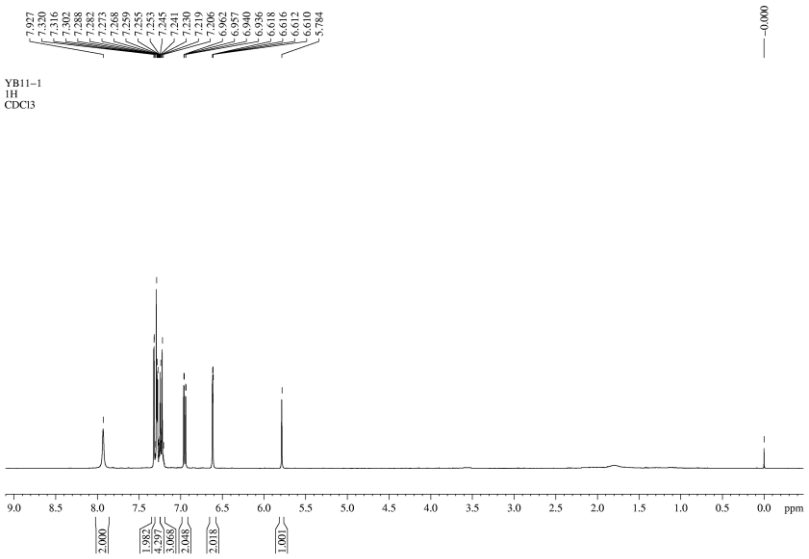

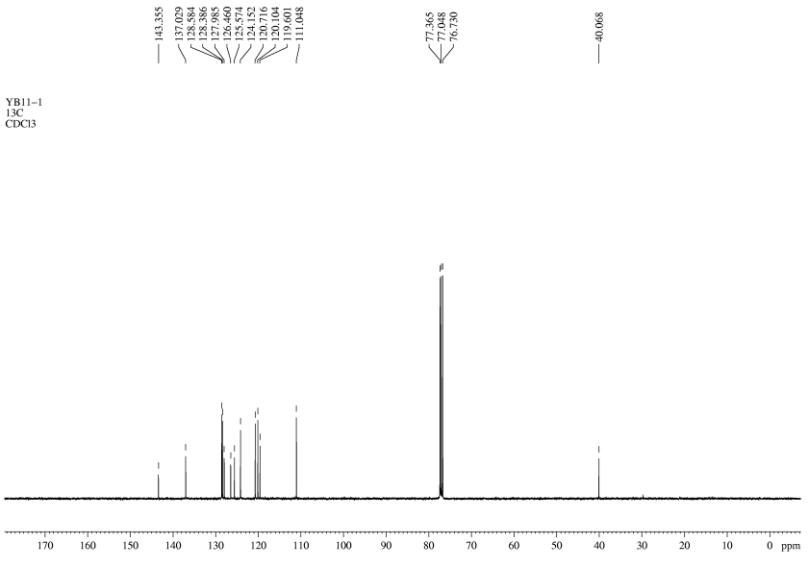

The ^{1}H-NMR and ^{13}C-NMR spectra of 3,3'-(phenylmethylene)bis(6-chloro-1H-indole)

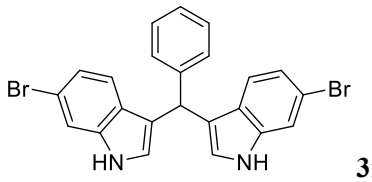

3n

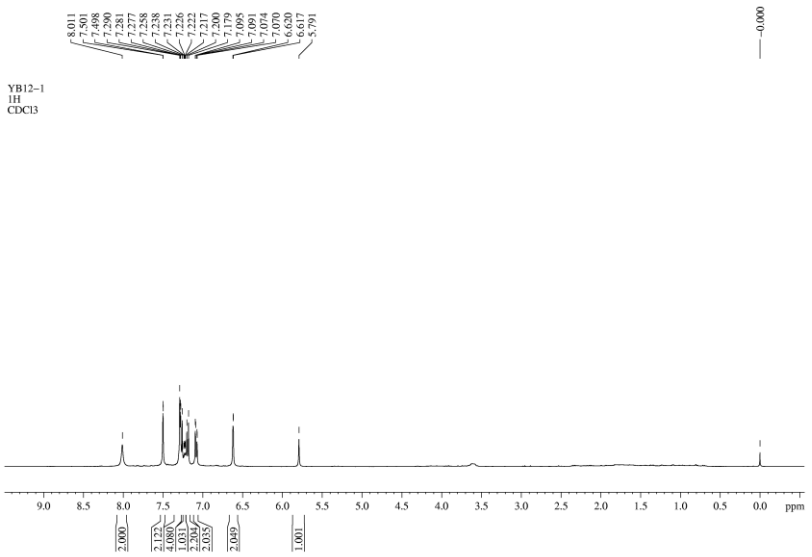

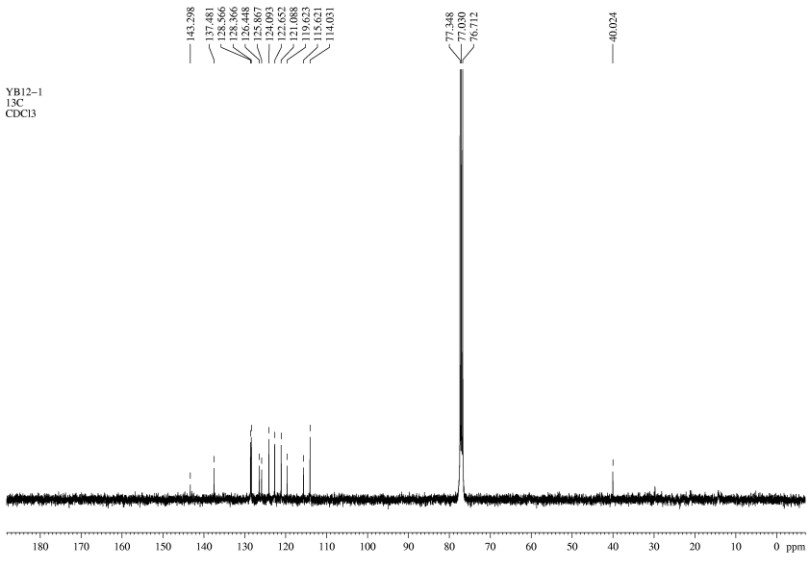

The ^{1}H-NMR and ^{13}C-NMR spectra of 3,3'-(phenylmethylene)bis(6-bromo-1H-indole)

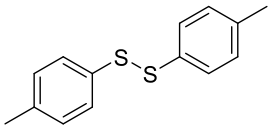

5a

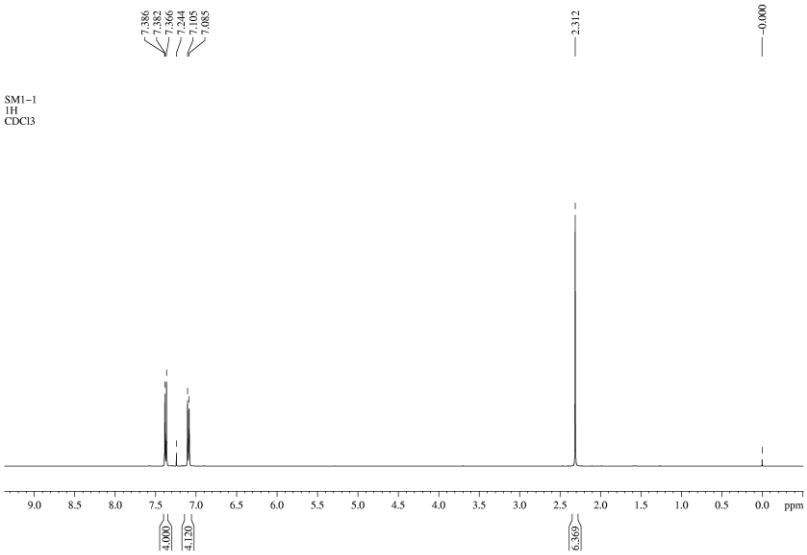

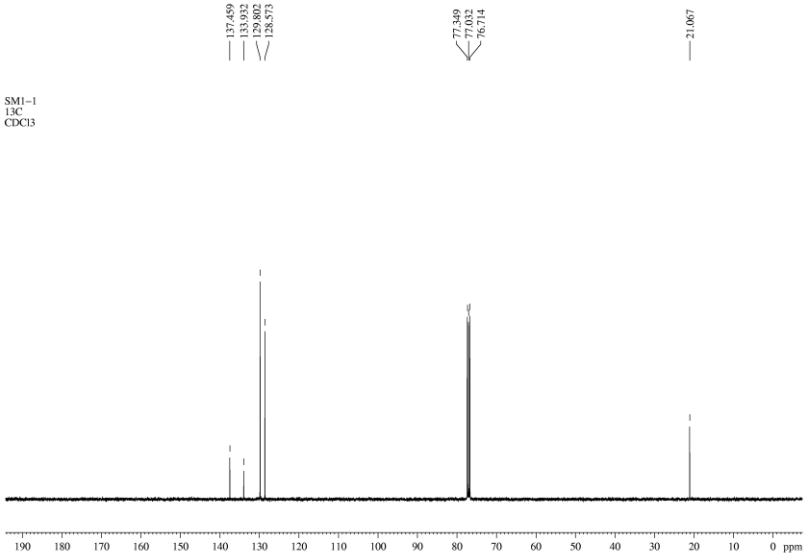

The ^{1}H-NMR and ^{13}C-NMR spectra of 4-methylphenyl disulfide.

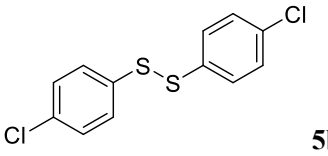

5b

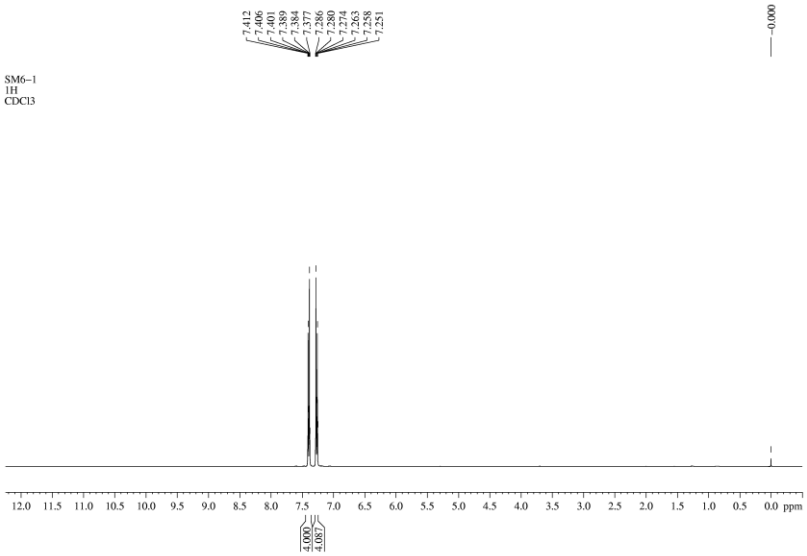

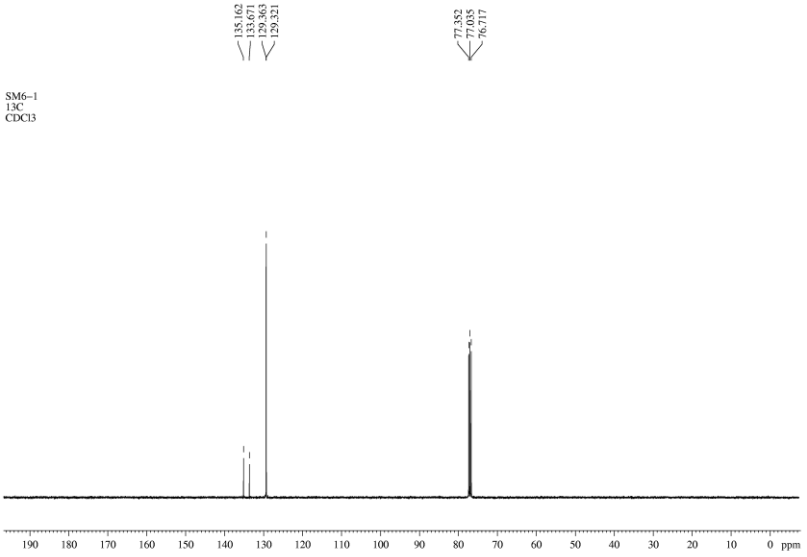

The ^{1}H-NMR and ^{13}C-NMR spectra of 4-chlorophenyl disulfide.

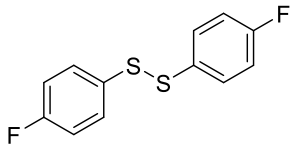

5c

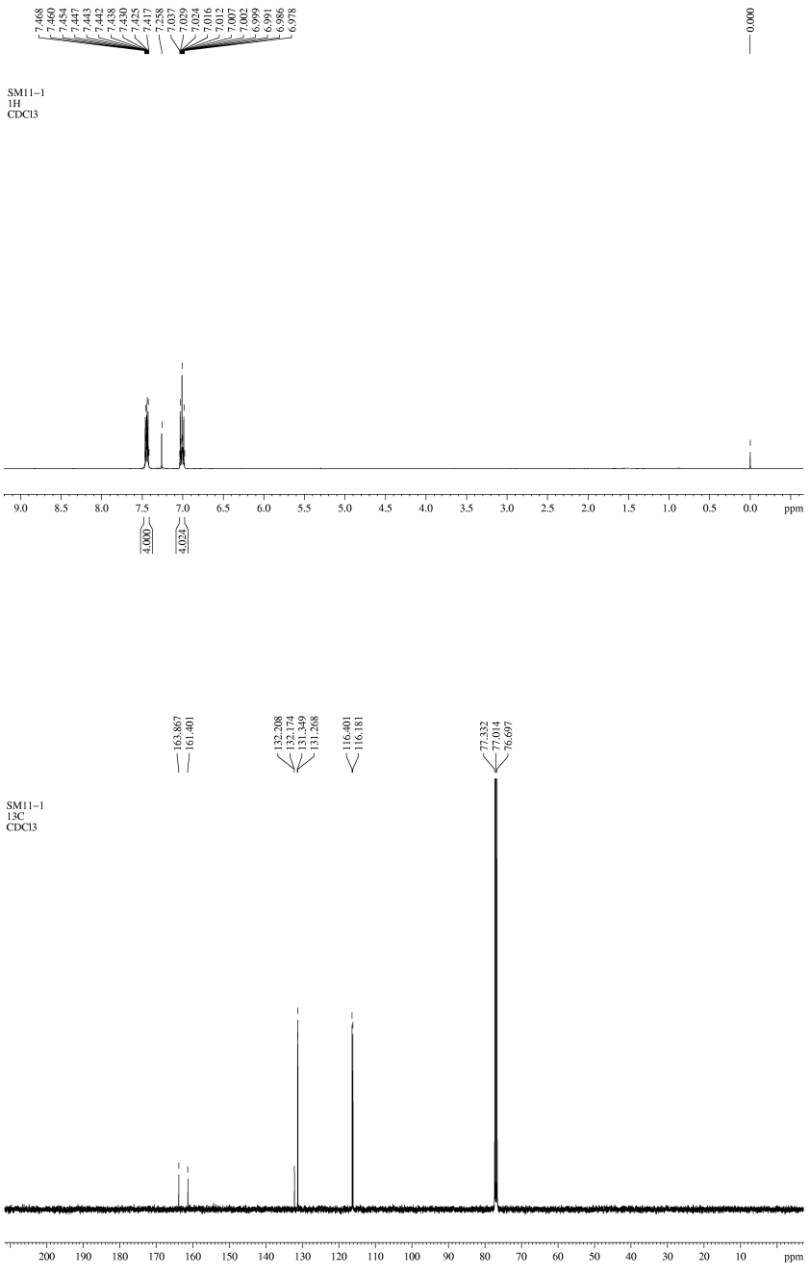

The ^{1}H-NMR and ^{13}C-NMR spectra of di-4-fluorophenyl sulfide

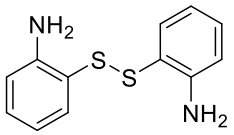

5d

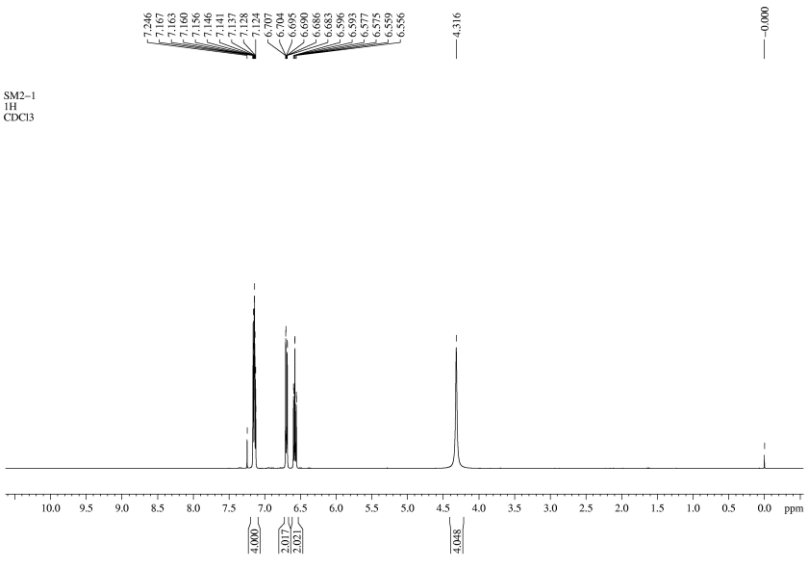

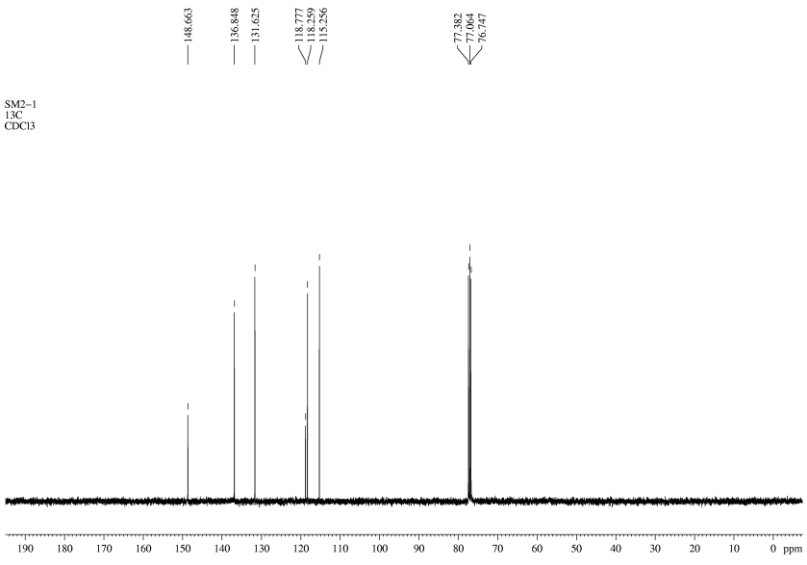

The ^{1}H-NMR and ^{13}C-NMR spectra of 2,2’-dithiobis(aniline)

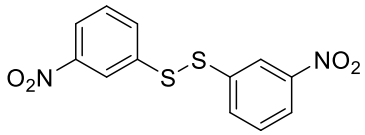

5e

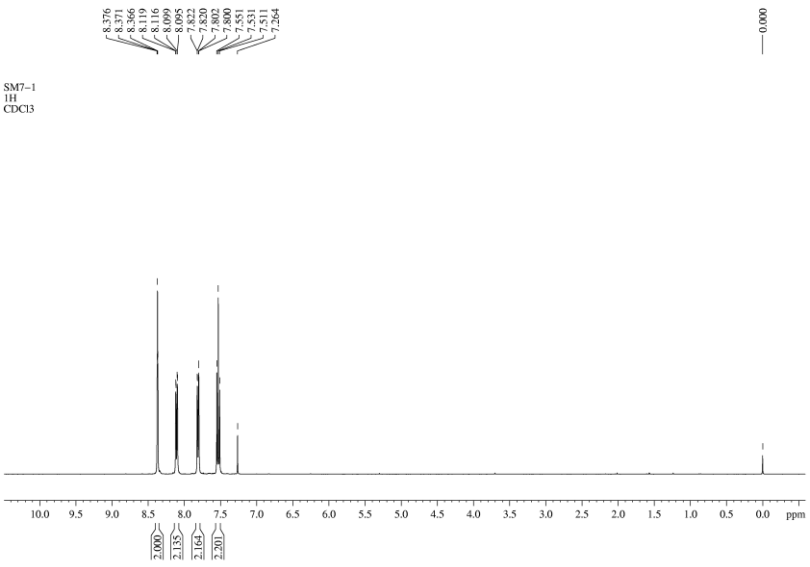

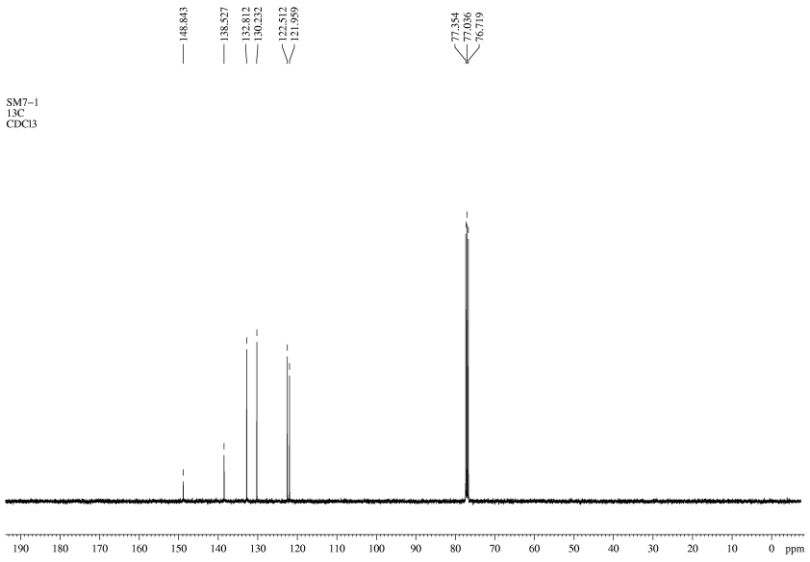

The ^{1}H-NMR and ^{13}C-NMR spectra of bis(3-nitrophenyl) persulfide

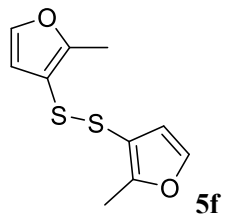

5f

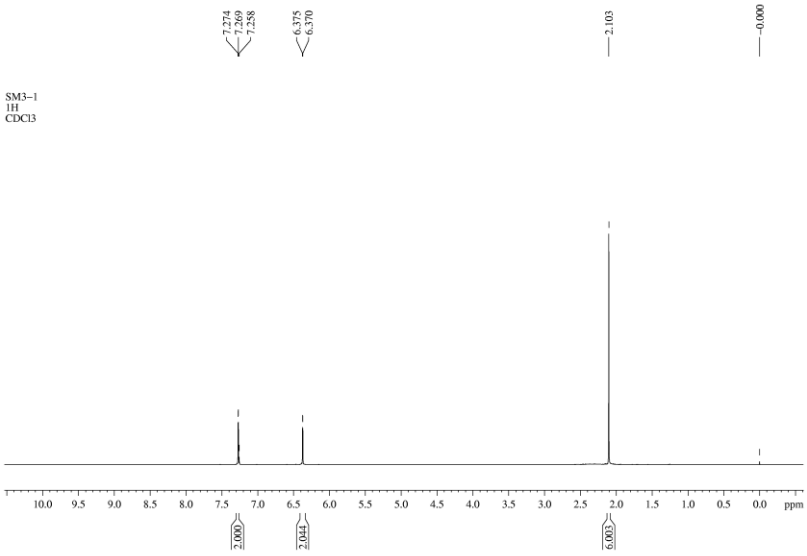

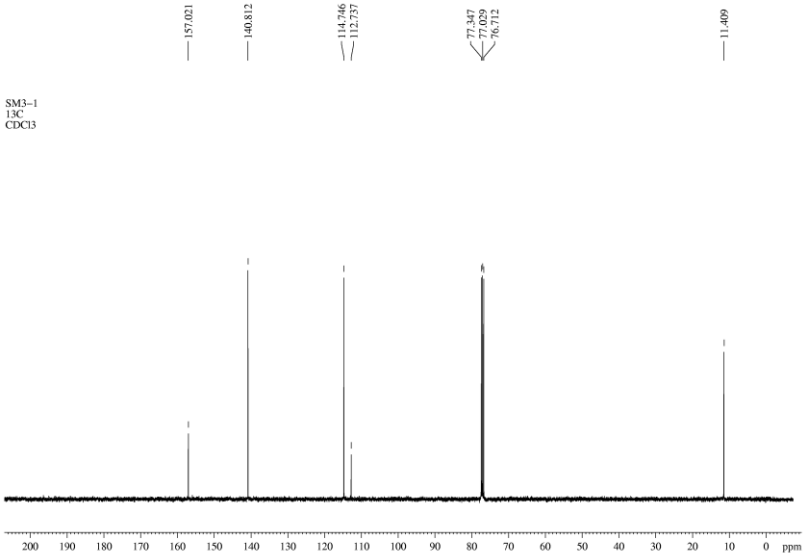

The ^{1}H-NMR and ^{13}C-NMR spectra of bis(2-methylfuryl) disulfide

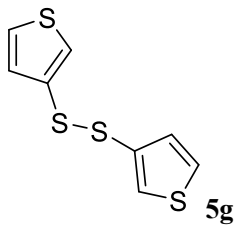

5g

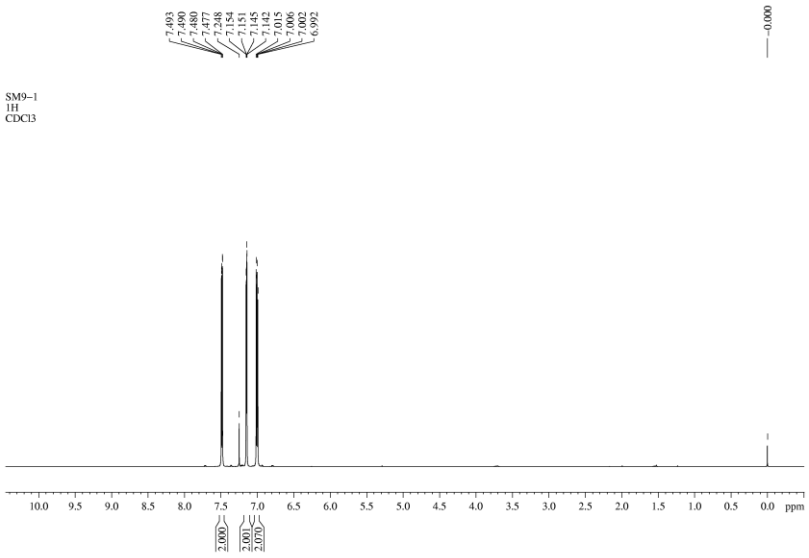

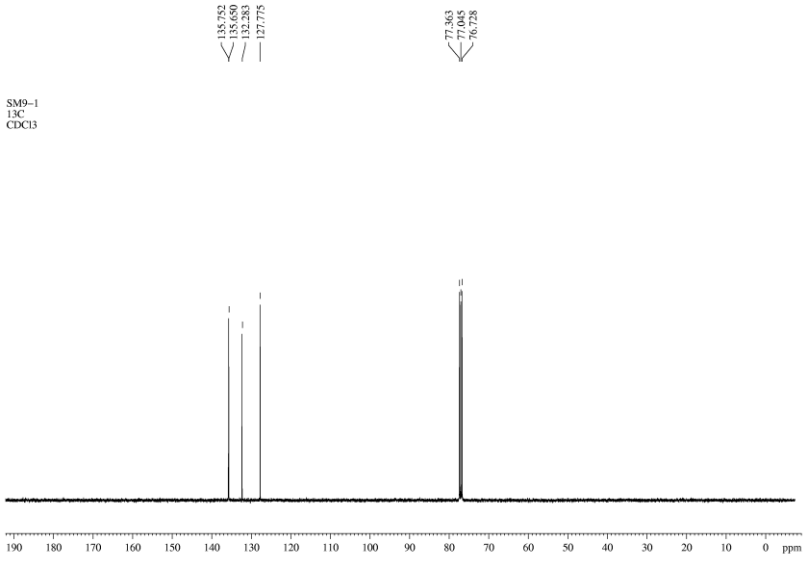

The ^{1}H-NMR and ^{13}C-NMR spectra of 2-thienyl

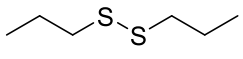

5h

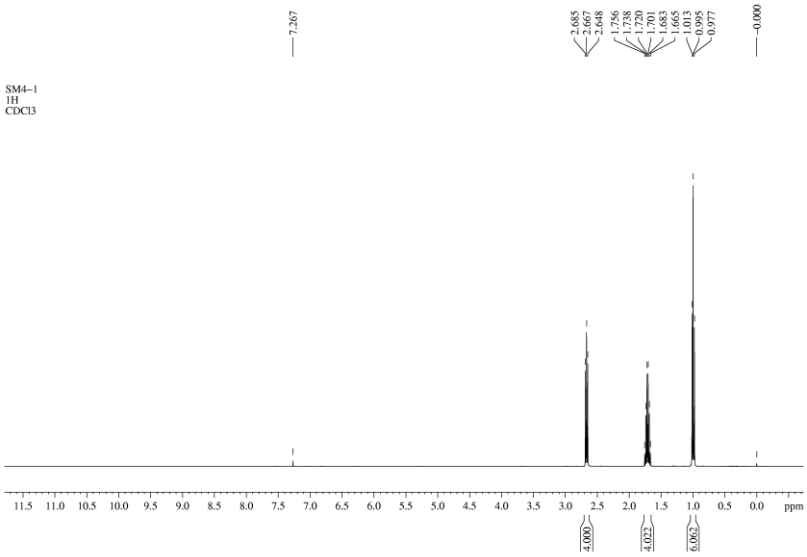

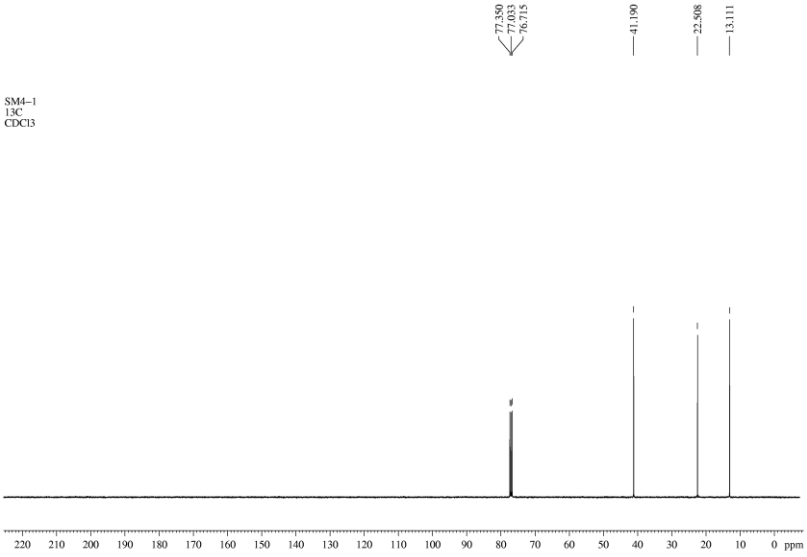

The ^{1}H-NMR and ^{13}C-NMR spectra of 4,5-dithiaoctane

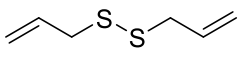

5i

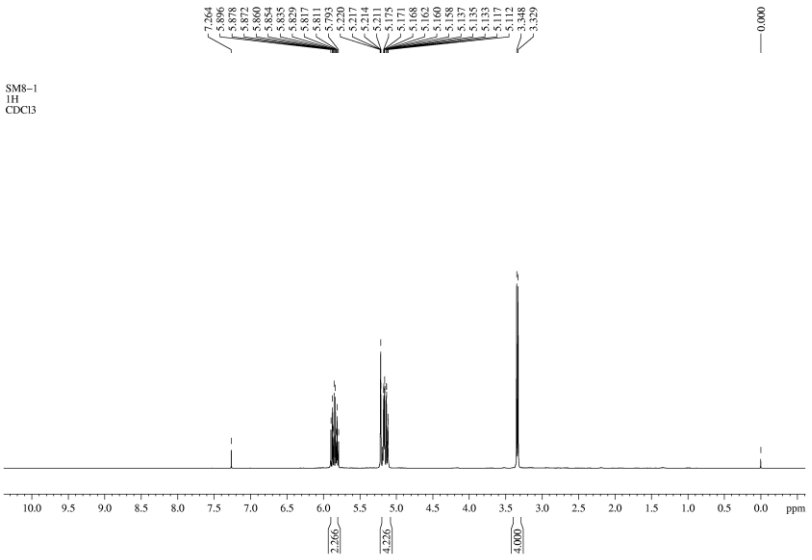

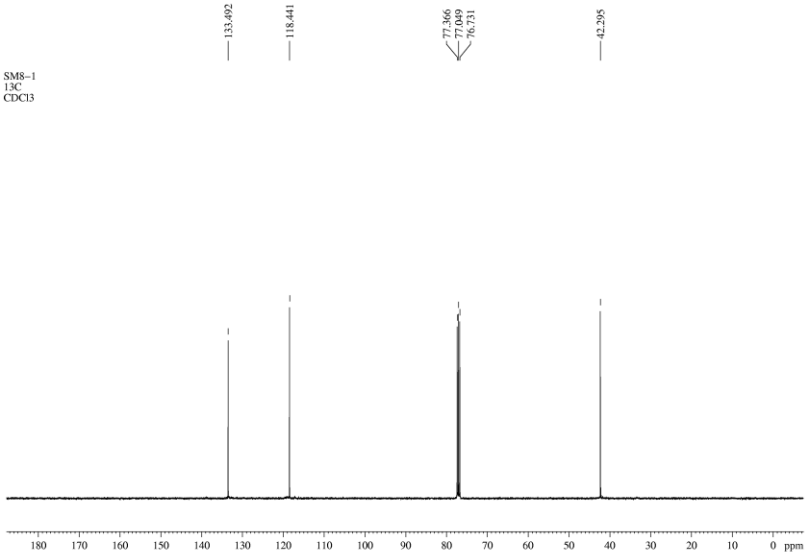

The ^{1}H-NMR and ^{13}C-NMR spectra of disulfide, di-2-propenyl

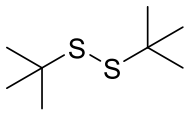

5j

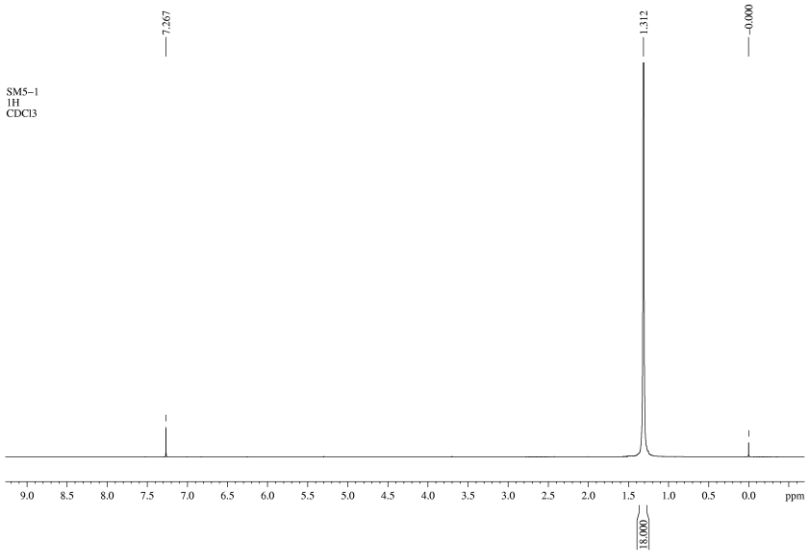

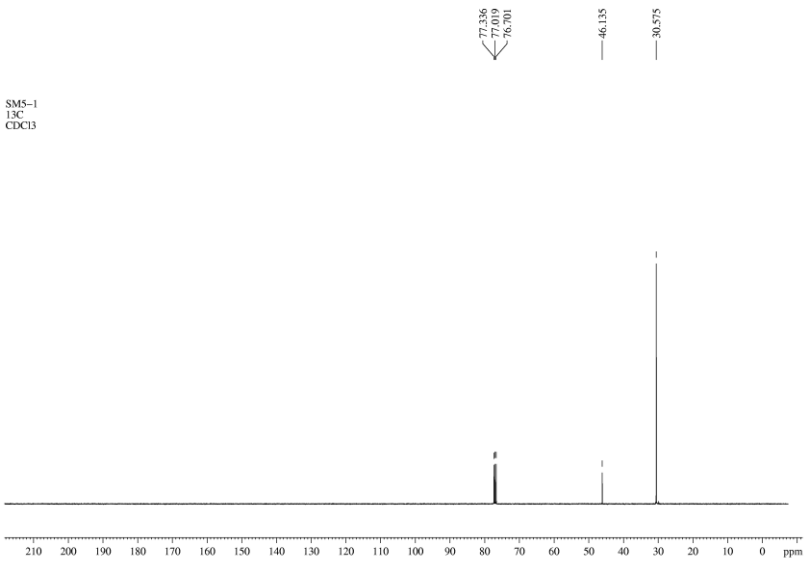

The ^{1}H-NMR and ^{13}C-NMR spectra of bis(1,1-dimethylethyl) persulfide

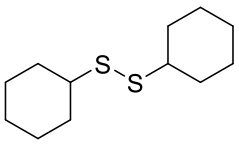

5k

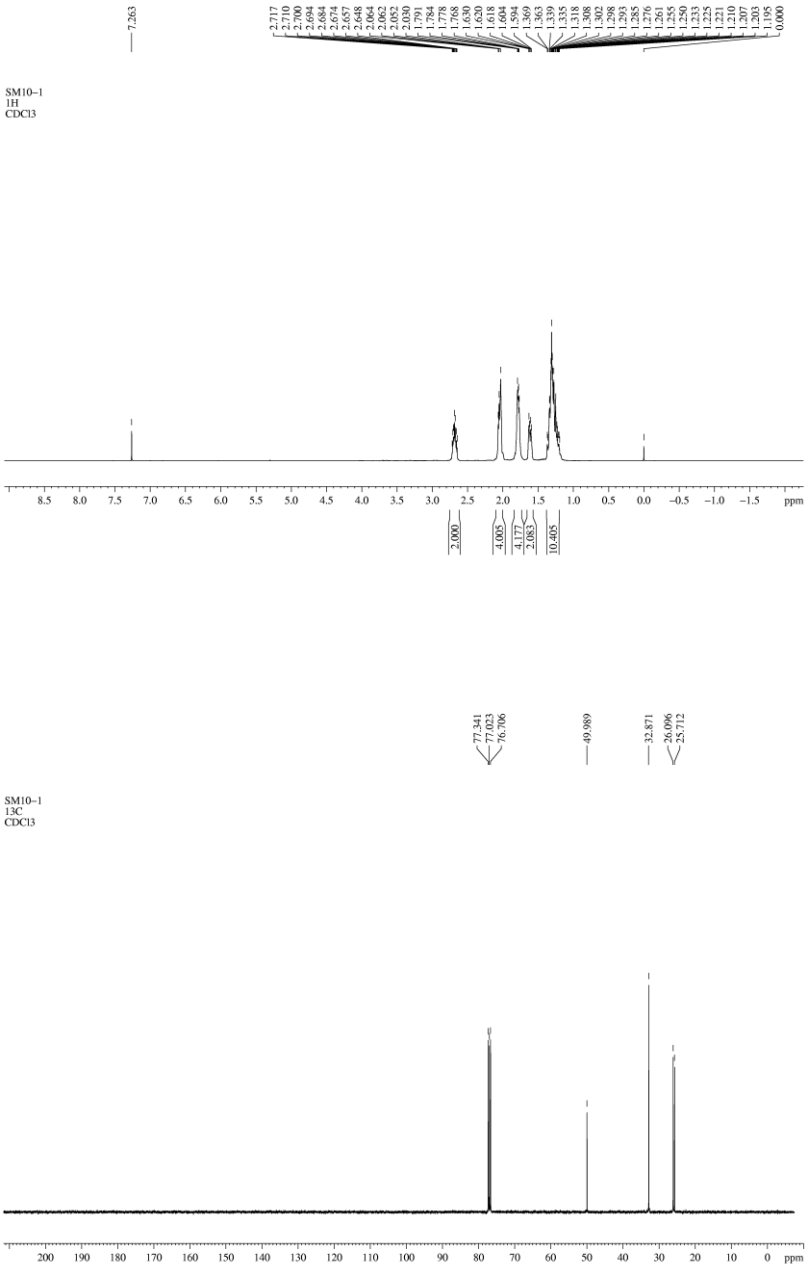

The ^{1}H-NMR and ^{13}C-NMR spectra of bis(cyclohexyl)disulfide

References

[1] Gaussian 16, Revision A.03, M. J. Frisch, G. W. Trucks, H. B. Schlegel, G. E. Scuseria, M. A. Robb, J. R. Cheeseman, G. Scalmani, V. Barone, G. A. Petersson, H. Nakatsuji, X. Li, M. Caricato, A. V. Marenich, J. Bloino, B. G. Janesko, R. Gomperts, B. Mennucci, H. P. Hratchian, J. V. Ortiz, A. F. Izmaylov, J. L. Sonnenberg, D. Williams-Young, F. Ding, F. Lipparini, F. Egidi, J. Goings, B. Peng, A. Petrone, T. Henderson, D. Ranasinghe, V. G. Zakrzewski, J. Gao, N. Rega, G. Zheng, W. Liang, M. Hada, M. Ehara, K. Toyota, R. Fukuda, J. Hasegawa, M. Ishida, T. Nakajima, Y. Honda, O. Kitao, H. Nakai, T. Vreven, K. Throssell, J. A. Montgomery, Jr., J. E. Peralta, F. Ogliaro, M. J. Bearpark, J. J. Heyd, E. N. Brothers, K. N. Kudin, V. N. Staroverov, T. A. Keith, R. Kobayashi, J. Normand, K. Raghavachari, A. P. Rendell, J. C. Burant, S. S. Iyengar, J. Tomasi, M. Cossi, J. M. Millam, M. Klene, C. Adamo, R. Cammi, J. W. Ochterski, R. L. Martin, K. Morokuma, O. Farkas, J. B. Foresman, and D. J. Fox, Gaussian, Inc., Wallingford CT, 2016.

[2] A.D. Becke, A new mixing of Hartree-Fock and local density-functional theories. J. Chem. Phys. 98 (1993) 1372-1377.

[3] P.J. Stephens, F.J. Devlin, C.F. Chabalowski, M.J. Frisch, Ab Initio calculation of vibrational absorption and circular dichroism spectra using density functional force fields. J. Chem. Phys. 98 (1994) 11623-11627.

[4] W.J. Hehre, R. Ditchfield, J.A. Pople, Self-consistent molecular orbital methods. XII. Further extensions of Gaussian-type basis sets for use in molecular orbital studies of organic molecules. J. Chem. Phys. 56 (1972) 2257-2261.

[5] S. Grimme, J. Antony, S. Ehrlich, H. Krieg, A consistent and accurate ab initio parametrization of density functional dispersion correction (DFT-D) for the 94 elements H-Pu. J. Chem. Phys. 132 (2010) 154104.

[6] T. Lu, F.W. Chen, Multiwfn: a multifunctional wave function analyzer. J. Comput. Chem. 33 (2012) 580-592.

[7] W. Humphrey, D, Andrew, K. Schulten, VMD: visual molecular dynamics. J. Mol. Graph. 14 (1996) 33-38.

[8] S. Manzettia, T. Lu, The geometry and electronic structure of Aristolochic acid: possible implications for a frozen resonance. J. Phys. Org. Chem. 26 (2013) 473-483.

[9] T. Lu, S. Manzettia, Wavefunction and reactivity study of benzo[a]pyrene diol epoxide and its enantiomeric forms. Struct. Chem. 25 (2014) 1521.

[10] M. Xu, J. Zhang, L. Liu, X. Cheng, J. Hu, Y. Sha, Z. Su, Y. Wang. $Co(NO_3)_2$/covalent organic framework nanoparticles for high-efficiency photocatalytic oxidation of thioanisole. Chemical Communications, 2022, 58(43):

6324-6327.

[11] H. He, X. Fang, D. Zhai, W. Zhou, Y. Li, W. Zhao, C. Liu, Z. Li, W. Deng A Porphyrin - Based Covalent Organic Framework for Metal - Free Photocatalytic Aerobic Oxidative Coupling of Amines. Chemistry-A European Journal, 2021, 27(58): 14390-14395.

[12] P. Li, X. Dong, Y. Zhang, X. Lang, C. Wang. An azine-linked 2D porphyrinic covalent organic framework for red light photocatalytic oxidative coupling of amines. Materials Today Chemistry, 2022, 25: 100953.

[13] M. Yang, S. Zhang, M. Zhang, Z. Li, Y. Liu, X. Liao, M. Lu, Y. Lan. Three-motif molecular junction type covalent organic frameworks for efficient photocatalytic aerobic oxidation. Journal of the American Chemical Society, 2024, 146(5): 3396-3404.

[14] S. Li, L. Li, Y. Li, L. Dai, C. Liu, Y. Liu, J. Li, J. Lv, P. Li, B. Wang. Fully conjugated donor – acceptor covalent organic frameworks for photocatalytic oxidative amine coupling and thioamide cyclization. ACS Catalysis, 2020, 10(15): 8717-8726.

[15] S. Liu, Q. Su, W. Qi, K. Luo, X. Sun, H. Ren, Q. Wu. Highly hydrophilic covalent organic frameworks as efficient and reusable photocatalysts for oxidative coupling of amines in aqueous solution. Catalysis Science & Technology, 2022, 12(9): 2837-2845.

[16] Z. Wu, X. Huang, X. Li, G. Hai, B. Li, G. Wang. Covalent-organic frameworks with keto-enol tautomerism for efficient photocatalytic oxidative coupling of amines to imines under visible light. Science China Chemistry, 2021, 64: 2169-2179.

[17] Q. Li, J. Wang, Y. Zhang, L. Sandoval, G. Bai, X. Lan. Structural and morphological engineering of benzothiadiazole-based covalent organic frameworks for visible light-driven oxidative coupling of amines. ACS Applied Materials & Interfaces, 2021, 13(33): 39291-39303.

[18] Adly M E, Mahmoud A M, El-Nassan H B. Green electrosynthesis of bis (indolyl) methane derivatives in deep eutectic solvents[J]. BMC chemistry, 2024, 18(1): 139.

[19] Yadav V, Balaraman E, Mhaske S B. Phosphine - Free Manganese (II) - Catalyst Enables Acceptorless Dehydrogenative Coupling of Alcohols with Indoles[J]. Advanced Synthesis & Catalysis, 2021, 363(18): 4430-4439.

[20] Nguyen N K, Ha M T, Bui H Y, et al. Magnetically recyclable CuFe2O4 catalyst for efficient synthesis of bis (indolyl) methanes using indoles and alcohols under mild condition[J]. Catalysis Communications, 2021, 149: 106240.

[21] Nguyen H T D, Nguyen T T, Nguyen P T K, et al. A highly active copper-based metal-organic framework catalyst for a friedel–crafts alkylation in the synthesis of bis (indolyl) methanes under ultrasound irradiation[J]. Arabian Journal of Chemistry, 2020, 13(1): 1377-1385.

[22] Hikawa H, Yokoyama Y. Pd-catalyzed C–H activation in water: synthesis of bis (indolyl) methanes from indoles and benzyl alcohols[J]. RSC advances, 2013, 3(4): 1061-1064.

[23] Liu X, Ma S, Toy P H. Halogen bond-catalyzed Friedel–Crafts reactions of aldehydes and ketones using a bidentate halogen bond donor catalyst: synthesis of symmetrical bis (indolyl) methanes[J]. Organic letters, 2019, 21(22): 9212-9216.

[24] Bahuguna A, Kumar S, Sharma V, et al. Nanocomposite of MoS2-RGO as facile, heterogeneous, recyclable, and highly efficient green catalyst for one-pot synthesis of indole alkaloids[J]. ACS Sustainable Chemistry & Engineering, 2017, 5(10): 8551-8567.

[25] Balgotra S, Kumar Verma P, Kour J, et al. A novel approach to access aryl iodides and disulfides via dehydrazination of arylhydrazines and arylsulfonylhydrazides[J]. ChemistrySelect, 2018, 3(10): 2800-2804.

[26] Yu X Z, Wei W L, Niu Y L, et al. Homocouplings of sodium arenesulfinates: selective access to symmetric diaryl sulfides and diaryl disulfides[J]. Molecules, 2022, 27(19): 6232.

[27] Wang G, Jia J, He Y, et al. Solid-state molecular oxygen activation using ball milling and a piezoelectric material for aerobic oxidation of thiols[J]. RSC advances, 2022, 12(29): 18407-18411.

[28] Xu X, Yan L, Huang W, et al. Facile and efficient transformation of thiols to disulfides via a radical pathway with N-anomeric amide[J]. RSC advances, 2024, 14(25): 17780-17784.

[29] Huber U A, Bergamin D. Novel Access to Furan-3-thiols and Derivatives, Impact Meat-Flavor Compounds[J]. Helvetica chimica acta, 1993, 76(7): 2528-2536.

[30] Wang J, Liu X, Yang S, et al. Controllable and chemo-selective conversion of sodium sulfinates to disulfides or thiosulfonates by a solvent-free mechanochemical approach[J]. Tetrahedron, 2023, 139: 133434.

[31] Khalili D, Iranpoor N, Firouzabadi H. 4, 4′-Azopyridine as an easily prepared and recyclable oxidant for synthesis of symmetrical disulfides from thiols or alkyl

halides (tosylates)/thiourea[J]. Journal of Sulfur Chemistry, 2015, 36(5): 544-555.

[32] Wang J X, Gao L, Huang D. A rapid and efficient synthesis of symmetrical disulfides under microwave irradiation conditions[J]. Synthetic communications, 2002, 32(7): 963-969.

[33] Spiliopoulou N, Kokotos C G. Photochemical metal-free aerobic oxidation of thiols to disulfides[J]. Green Chemistry, 2021, 23(1): 546-551.